We are IntechOpen, the world's leading publisher of Open Access books Built by scientists, for scientists

4,800
Open access books available

122,000
International authors and editors

135M
Downloads

Our authors are among the

154
Countries delivered to

TOP 1%
most cited scientists

12.2%
Contributors from top 500 universities

CLARIVATE ANALYTICS BOOK CITATION INDEX INDEXED

WEB OF SCIENCE™

Selection of our books indexed in the Book Citation Index in Web of Science™ Core Collection (BKCI)

Interested in publishing with us?
Contact book.department@intechopen.com

Numbers displayed above are based on latest data collected.
For more information visit www.intechopen.com

12

Organic Molecules on Noble Metal Surfaces: The Role of the Interface

Maddalena Pedio[1], Cinzia Cepek[1] and Roberto Felici[2]
[1]*IOM CNR, Laboratorio TASC Area Science Park, Basovizza Trieste*
[2]*ESRF Grenoble*
[1]*Italy*
[2]*France*

1. Introduction

Among the new developments in the use of noble metals, the organic-inorganic systems formed by Self Assembled Molecular (SAM) layering on noble metal surfaces represent a main topic. In this chapter we discuss the use of complementary surface science techniques Applied to these sysems. Our aim is to give an overview on our recent case studies of organic molecular layers interacting with noble metal surfaces. Functionalized molecular assembled films are important in many application fields, ranging from sensors and photovoltaic cells to nanostructured devices. In microelectronics adsorbed organic molecules on metal surfaces are a subject of intensive investigation, due to the fundamental interest in interfacial coordination chemistry and its many potential applications. Physical details and morphology, together with the grain size, orientation of the molecules in the film and the concentration of defects, play a crucial role in device performances, since they determine the carrier injection properties.

In particular we discuss how the adsorption of organic molecules can induce strong or weak perturbation of the noble metal substrates whose characterization is necessary for the control of the modified electronic properties with SAM-noble metal interfaces. These systems are complicated by the fact that the molecule-substrate system must be taken into account as a whole and it is not possible to simply transfer molecular functionalities, deduced in their isolated state, to the adsorbed case. The metal surface can force the molecule to rearrange its internal structure (leading to complex structural deformation of the adsorbed molecules) and the metal surface lattice plays an important role aligning the assembling with the main lattice directions. The mechanism of conjugated molecule ordering and (in some case) anchoring on surfaces is due to a balance of intermolecular binding forces and of molecule-substrate interaction involving a large number of sites. In case of strong bond, this can result in either displacive substrate reconstructions, involving extensive mass transport and the formation of ordered arrays of nanodimples.

Noble metal surfaces are valuable substrates for SAM because of their low chemical reactivity together with high atomic surface mobility resulting in the capability of reordering after molecular deposition. The high electron density at the crystal surface

provides a charge reservoir. Comparisons of the different organic-metal surface combinations will be discussed, focussing on the role of the substrate moieties.

2. Research methods

The complexity of the organic molecules deposited onto noble metal surfaces deserves a multi-techniques approach. Our methodology is focussed on the interrelation between electronic properties and structural profiles. Electron Spectroscopies, Photoemission Electron Spectroscopy (PES) and Inverse Photoemission Spectroscopy (IPS) and X-ray Absorption Spectroscopy (XAS) are widely used, in campus and synchrotron radiation facitilies, to characterize the electronic properties of condensed matter and are successfully applied to low dimensional systems. The richness of information achievable with these techniques make them extremely useful for the fine characterization of organic-inorganic interfaces and Self Assembled Monolayer systems. These techniques are complementary to Scanning Microscopies (in particular Scanning Tunnelling Microscopy, STM) and Diffraction techniques Low Energy Electron Diffraction, (LEED), Helium Scattering, (HAS) and Surface X-ray Diffraction, (SXRD). Imaging through STM offers the access to details of the surface topography at atomic resolution and in particular cases to information about the Density of States (DOS) across the Fermi level by the Scanning Tunneling Spectroscopy (STS). Diffraction techniques provide structural details of the surface and (even buried) interfaces. In the following we shortly describe the main information provided by selected research methods. We address the reader to more complete reviews and text books (as for example Luth1994, Hufner1995, Feidenhans'l 1989, Woodruff 1988, Robinson1992, Besenbacher 1996, Chen1993).

2.1 Introduction to surface x-ray diffraction

Radiation can interact with matter in two ways: it can be diffused elastically and then the coherent sum of all the waves diffused by the single objects sum coherently giving diffraction, or it can induce (electronic, vibrational, and rotational) transitions in the atoms and molecules it interacts with. Diffraction is extremely important for the determination of the structural properties of matter being an interferometric technique sensitive to the relative positions of the scattering objects.

SXRD is usually applied to ordered samples. This technique provides information on the structure of both the terminating layers of the ordered substrate lattice or of an ordered new structure which is formed at the surface. In the first case, the basis of SXRD is the measurement of the diffracted intensity raising from the termination of the periodic bulk structure which is located along rods in the reciprocal space having their origin at the Bragg points of the bulk structure (Robinson 1986). These rods, which are perpendicular to the terminating surface, are usually referred as Crystal Truncation Rods (CTRs). In the second case the diffracted intensity is along continuous rods, still perpendicular to the surface with an in plane periodicity defined by the surface unit cell. If the surface unit cell is due to a reconstruction of the bulk cells and then it has in-plane dimensions which are commensurate with the bulk unit cell, the associated rods take the name of Fractional Order Rods (FORs) (Feidenhans'l1989). A measurement of the intensity of both the CTRs and FORs as a function of the continuous variable l, which is the reciprocal space coordinate perpendicular to the scattering surface, provides information on the expansion or

contraction of the top layers of the substrate, on the substrate roughness and on the in plane position of all the atoms belonging to the surface unit cell.

X-rays interacts weakly with matter and the scattering process can be well described in the distorted Born approximation. This makes the data analysis quite simple because all the terms describing multiples scattering events can be neglected. In the case of ordered samples we can use the same approach normally employed in bulk crystallography. Among the different quantities it is important to highlight the role of the Patterson map obtained by Fourier transformation of the intensity of the fractional order rods at $l \approx 0$. In this case the map is the autocorrelation function of the electron density projected onto the surface. It usually provides hints on the main correlation vectors present in the unit cell. Because the unit cell is larger and commensurate with the bulk unit cell the atoms which have not moved from their ideal bulk termination position will not appear in the Patterson (Feidenhans'l, 1989).

The fitting of the data can be carried out using the ROD program (Vlieg, 2000). To gather sensitivity to a particular atomic species, all the above techniques can also be coupled to energy scans through absorption edges. In the simple case the change in the atomic scattering power at the resonance will give the possibility of determining the contribution of a particular atomic specie to the scattered intensity (Benfatto & Felici 2001). X-ray diffraction presents the advantage of being able to observe the buried interface even when it is covered by a thick layer of adsorbed molecules giving the opportunity of determining the substrate structure during the different growth phases.

2.2 Basic principles of scanning tunneling microscopy and scanning tunneling spectroscopy

Since the discovery the STM (Binnig and Rohrer) has revolutionised the field of surface science, making possible real space atomic resolution images of a sample surface. In STM measurements a fine pointed tip is brought extremely close to a surface and a voltage is placed between the tip and the sample surface. In this condition a tunneling current can exist between the tip and surface. The current flow is very sensitive to the distance between tip and surface. The tip can be rastered across the surface with the aid of piezo-electric actuators. The current travelling between the sample and tip is sensed and the tip is moved towards and away from the sample surface, keeping the current flow constant. Obviously, the sample needs to be electrically conducting, and to achieve atomic resolution for most samples the STM needs to operate in Ultra High Vacuum (UHV) conditions. Basics of STM and STS can be found in many reviews (Besembacher1996, Chen 1993, Gavioli2008 and refs therein).

STM is one of the most powerful tools for observing surfaces, adsorbates and molecular structures at nano scale level and a wealth of study using STM as main tool are present in the literature. STM and STS have found a wide range of applications, providing not only topographic details of the surfaces but the electron density distribution. The key of the measurement information is the tunneling matrix element, which depends explicitly from the sample and tip wave functions. Since the atomic structure of the tip is usually not known, one needs to model the tip wave function to understand the information provided by the tunneling current. Assuming a tip with radius R and an s-type only (quantum

numbers $l \neq 0$ neglected) wave functions and small applied bias voltage, the current results to be

$$I \propto U \cdot n_t(E_F) \cdot e^{2xR} \sum_{\mu\nu} \left|\psi_\nu(r_0^2)\right|^2 \delta(E_\nu - E_F) \tag{1}$$

where E_F is the Fermi energy, r_0 is the center of curvature of the tip, $n_t(E_F)$ is the density of states at the Fermi level for the tip, and the decay rate $x = (2m\phi)^{1/2}/\hbar$ depends on the effective potential barrier height ϕ. The quantity

$$n_s(E_F, r_0) = \sum_{\mu\nu} \left|\psi_\nu(r_0^2)\right|^2 \delta(E_\nu - E_F) \tag{2}$$

is the charge density of the electronic states at the Fermi level (Tersoff1983, Tersoff1985 in Gavioli2008), i.e. the surface local density of states (LDOS) at E_F, evaluated at the center of curvature of the tip. The interpretation of the tunneling current as contour map of the surface LDOS is limited to small applied bias (less than 0.5 V) and ignores the angular dependence of tip wave functions.

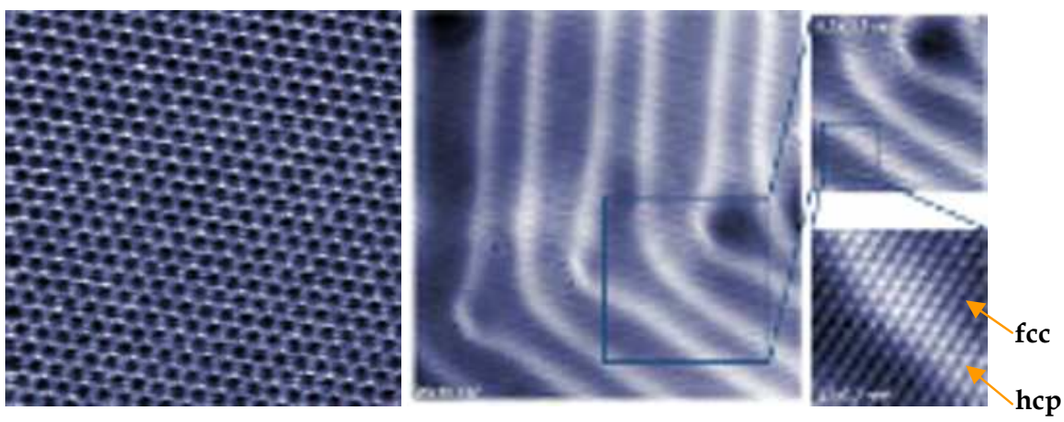

Fig. 1. a) Atomically resolved Cu(111) surface in constant height mode T=5K, 4.5x5 nm2 Omicron LT-SPM/Qplus Dr. B.Such, group Prof. E.Meyer, Univ. Basel, Swi. b) Ultrahigh resolution (2048x2048 pixels) topographical image of Au(111) reconstruction, 26x26 nm2, 40pA, 200mV, 4K SPECS Joule-Thomson STM Prof. W.Wulfhekel, Karlsruhe, Germany (web site http://www.specszurich.com/en/image_gallery_content---1--1122.html)

Figure 1 shows two examples the STM images of the Cu(111) and Au(111) surfaces. Gold presents the herringbone reconstruction with periodicity √3x23 (see description in section 3) formed by alternate hcp (clearer atoms) and fcc regions (dark). These topographic atomic resolved images give an idea of the power of high resolution of STM topography. Nevertheless STM images do not contain direct information on the absorption site and the configuration at the interface could only be inferred. More realistic assumption must be taken into account to interpret the imaging and the data of STM (Chen1990). The assignment of the atomically resolved structures should be taken with care, with a comparison to *ab-initio* calculations of the electronic structure or comparison to other experimental techniques.

2.3 Introduction to photoemission (valence photoemission UPS and core level photoemission XPS), inverse photoemission IPS and absorption (XAS)

Electron Spectroscopies, are precious tools for the fine characterization of organic-inorganic interfaces. They give access to the density of electronic empty and filled states (or bonding and antibonding orbitals of molecules) providing information on the electronic configuration, the molecule-metal surface bond, the effect of charge transfer, energy level alignment at interfaces and the orbital modification of the adlayer structures. This ensemble of information is fundamental, as we will discuss in section 4, for organic-inorganic systems, whose physical and structural fine details play a crucial role, in their properties and technological applications.

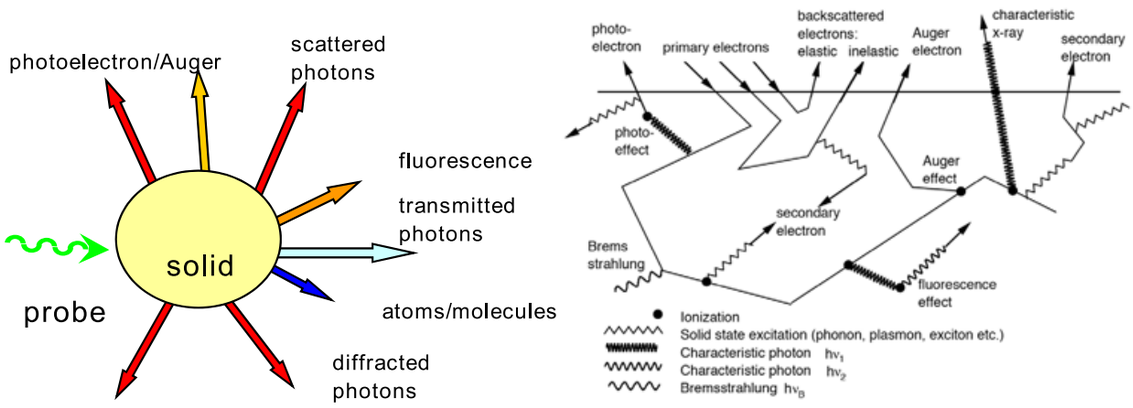

Perturbation-Excitation-Response

Fig. 2. Left: In a spectroscopic experiment the incoming probe (photons, electrons) interacts with the sample and produces different outgoing probes, depending on the different interaction processes each with its proper cross section σ; Right: possible processes inside a solid induced by an electron beam (Werner, 2005)

A spectroscopy experiment can be rationalized in three steps: Incoming probe onto a sample, Excitation inside the sample induced by the probe perturbation, detection of the outgoing response. When a photon (or electron) beam interacts with condensed matter, the products of such interaction compose different response channels. Therefore an electron spectroscopy experiment can be considered as a scattering (elastic or anelastic) experiment where a beam of electrons, or photons (UV, Soft or X-rays) impinging onto the system with prescribed energy and momentum, perturbs the sample, inducing its proper excitations or transitions that involve the eigenstate of the sample. Measuring the energy and momentum of the outgoing probes (emitted or absorbed X-rays or electrons) provides the "response" spectrum. Electron spectroscopies treated here, are in linear response regime, i.e., the interaction (photons-matter or electrons-matter) only weakly perturbs the system under study.

Examples of physical processes occuring when an electron (or a photon) interacts with a solid surface are presented schematically in the Figure 2 left (Werner, 2005). When the incoming electron is sufficiently energetic, a wealth of phenomena can take place leading to different types of emitted particles: elastically and inelastically backscattered electrons, exciton, phonon, plasmon excitations, photoelectrons, Auger recombination of a hole left by the photoelectron, fluorescence recombination and the so-called secondary electrons.

The information of the experiment is contained in the differential cross section $\frac{d\sigma(E)}{dVd\Omega}$ (V=volume, E energy, Ω solid angle of detection), and strongly depends on the experimental geometry adopted in the experiment, the properties of the incoming probe, the kind of detector, the angle of detection ecc., all quantities which can be modelled. The cross section σ of the excitation process, has the dimension of an *area* (namely is defined in barn= 10^{-24} cm^2) and is related to the transition probability of the interaction process. For each channel the σ (Hüfner1995, Woodruff1988, Bassani1983) can be expressed in terms of interaction probability W_{if} from the initial (wavefunction ψ_i, initial energy E_i) to the final (ψ_f initial energy E_f) states by using: a) the first order of the perturbation theory (with the assumptions of a weak perturbing probe), b) the single particle approximation (the final state approximate the ground state with only one particle passed from i to f state) c) the dipole approximation (that assumes that the wavelength of the radiation is large compared to the dimensions of the excitation volume).

$$\frac{d\sigma}{dVd\Omega} \propto \sum_{if} W_{if} \; ; \; W_{i\to f} \propto \frac{2\pi}{\hbar}\left|\left\langle \psi_f \left| r \right| \psi_i \right\rangle\right|^2 \delta(E_f - E_i - h\nu) \tag{3}$$

The quantity in bracket provides the density of states of the sample, the delta function implies the energy conservation, hν is the photon energy.

In this way, the measured flux of absorbed or emitted particles, as a function of energy and angle, can be compared with the calculated interaction probability, as for example the current density of photoelectrons, or the absorption of photons as a function of the photon energy etc. A rigorous treatment of the cross section calculation for the different electron spectroscopies is beyond the scopes of this chapter and we address the reader to manual and books for a deeper treatment (see for example Bassani1983, Hüfner1995, Lüth1995).

The schematics of the processes discussed in the following are shown in fig. 3: photoemission (PES, for historical reason the core level photoemission is called often X-ray Photoemission Spectrscopy XPS while valence band photoemission Ultraviolet Photoemission Spectroscopy UPS), Inverse Photoemission (IPS) and X-ray Absorption spectroscopy spectroscopies. PES corresponds to an the photoelectron initially in a core level (X-ray Photoelectron Spectroscopy XPS), or a valence band level (Ultraviolet Photoelectron Spectroscopy UPS), XAS from elemental edge corresponds to the absorption of the impinging photon by a core level electron, IPS technique involves the detection of photons emitted by the decay of an impinging electron from a level above the Vacuum Level to an empty electron state of the sample.

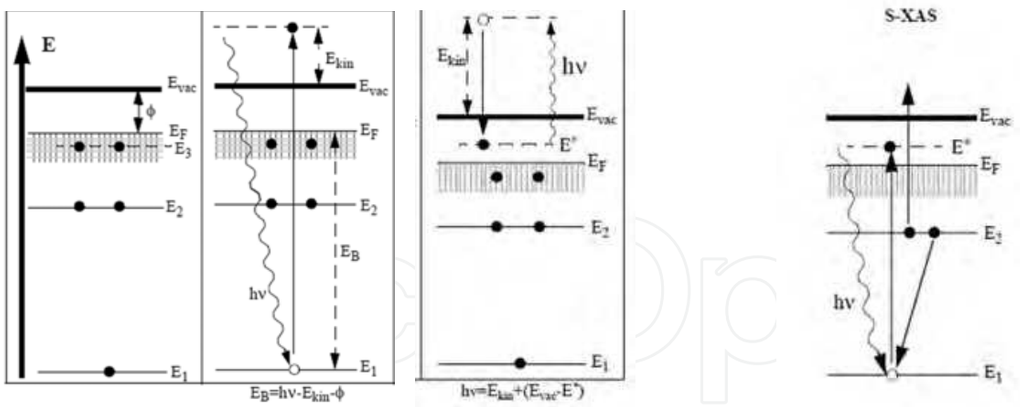

a) Ground State b) PES c) IPS d) XAS and Auger recombination

Fig. 3. Energy levels and processes of photoemission and absorption. A metal in a ground state (left panel) Evac indicates the vacuum level, ϕ the work function that is the energy between the Fermi level EF and the Evac, the E1 and E2 are proper energy levels of the sample. In Photoemission a photon with energy hv > E1-Evac promotes a photon above the Evac, leaving a hole in the state E1. In Inverse Photoemission an impinging electron makes a transition from the energy level above the Evac and an empty state E* inducing the emission of a photon, in absorption an impinging photon is absorbed leaving a core hole in the level E1 and the recombination produces either a fluorescence decay or an Auger electron.

2.3.1 NEXAFS

X-ray Absorption Spectroscopy (XAS) combined with synchrotron radiation is a well-established technique that provides information on the electronic, structural and magnetic properties of matter. In X-ray absorption, a photon is absorbed by the atom, leading to the transition of an electron from a core state to an empty state above the Fermi level. The absorption cross-section is proportional to the absorption coefficient and depends on the energy and on the measured element. To excite an electron in a given core-level, the photon energy has to be equal or higher than the binding energy of this core-level. This gives rise to the opening of a new absorption channel when the photon energy is scanned from below to above this core-level energy. The energies of the absorption edges therefore correspond to the transition from the core-level energies to the empty states and are characteristic for each element, making X-ray absorption an element-selective technique.

The fine structure above the x-ray absorption edge of a core level can be separated into a *n*ear-*e*dge region (Near Edge X-ray Absorption Fine Structure, NEXAFS, Another acronym used in the literature is XANES) (Stöhr1992), which is located within ≈ 30 eV above the edge, and an *e*xtended region at higher photon energies (Extended X-ray Absorption Fine Structure, EXAFS). Due to the small inelastic mean free path of the photoelectrons in the respective energy range, NEXAFS is dominated by multiple scattering, in contrast to EXAFS, where the photoelectron interacts with the surrounding atoms by single scattering events. On the other hand the near edge provides information of the cross section of the element selective density of final empty states, which for molecules are the directional antibonding π molecular states. An example is reported in figure 4 right. The photon absorption is

controlled by dipole selection rules, which lead to general relations for the angle-dependence of the resonance intensities [Stohr, 1992].

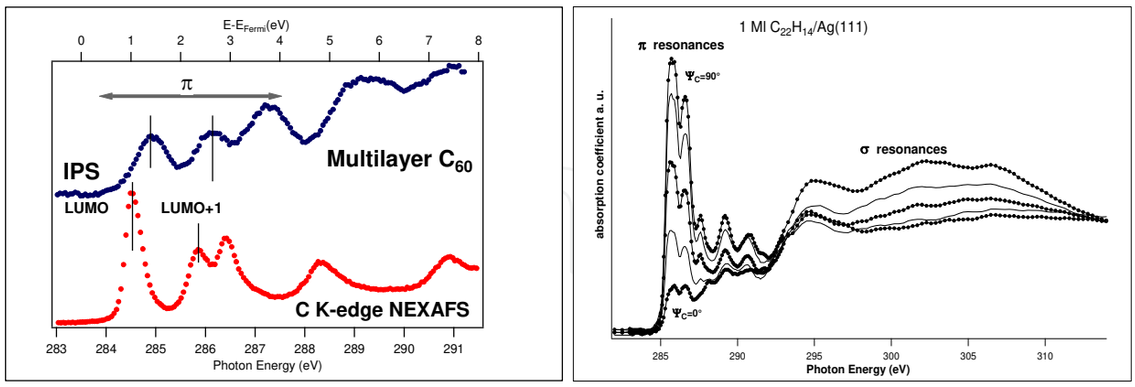

Fig. 4. Left: C Kedge NEXAFS of C_{60} multilayer compared with Inverse Photoemission (Felici 2009). Right: Example of C Kedge NEXAFS of the linear molecule Pentacene ($C_{22}H_{14}$) deposited (1ML) onto Ag(111) measured varying Electric field vector of the incident synchrotron light (Pedio 2007).

Making use of the polarized nature of the synchrotron radiation the orientation, relative to the surface of the molecular orbitals of an adsorbed molecule , can be determined. For this reason NEXAFS is mostly used to determine molecular orientations by observing the polarization dependence of the resonance intensity, which is mainly controlled by well-established symmetry selection rules. Figure 5 left) shows an example of the C kedge of C_{60} molecular films. The signals in the NEXAFS region can be divided into π and σ resonances. The lower energy π resonances are assigned to transitions from the core level into an unoccupied molecular orbital of (local) π symmetry that lies below the vacuum level, while the σ lie above. Thus, the NEXAFS spectroscopy probes empty levels below the ionization threshold, similarly to IPS (see next paragraph), but due to the absorption process, the final system has an electron less (N-1) and a hole in the core level. Note the differences of the energy separation of the peaks in the two spectra in Figure 4 left, due to the presence of the C1s core hole in the absorption process. Specifically Density Functional Theory (DFT) can reproduce the NEXAFS spectrum of the excited state (presence of the core hole) of molecules, either in the gas phase or in solid thin films, providing the oscillator strengths and the intensities (Triguero 1998,). The ground state is nicely reproduced by ground state DFT calculation (absence of the hole). For more details see (Brühweilr2002, Felici, 2009).

2.3.2 Photoemission

Photoemission spectroscopy (PES) is based on the photoelectric effect, which is the process of extracting an electron by means of an impinging photon with energy greater than the electron binding energy. PES measures, in its simpler version, the kinetic energy distribution of photoelectrons, which are emitted from a sample, when it is irradiated with monochromatic light. The energy of the photoelectrons leaving the sample is determined using an analyser that selects the kinetic energies of the photoelectrons and measures their intensity. This gives a spectrum with a series of photoelectron peaks. Within a single particle picture, the kinetic energy distribution of the detected electrons mimics the distribution in energy of the occupied

electron states in the ground state (see Fig.5 left). In this case, the kinetic energy E_k of the photoelectron coming out from the sample is approximately given from the following relation:

$$E_k = h\nu - E_b - \Phi_A \tag{4}$$

where E_b is the binding energy of the photoelectron relative to the Fermi level, hν the used photon energy and Φ_A is the work function of the electron analyzer.

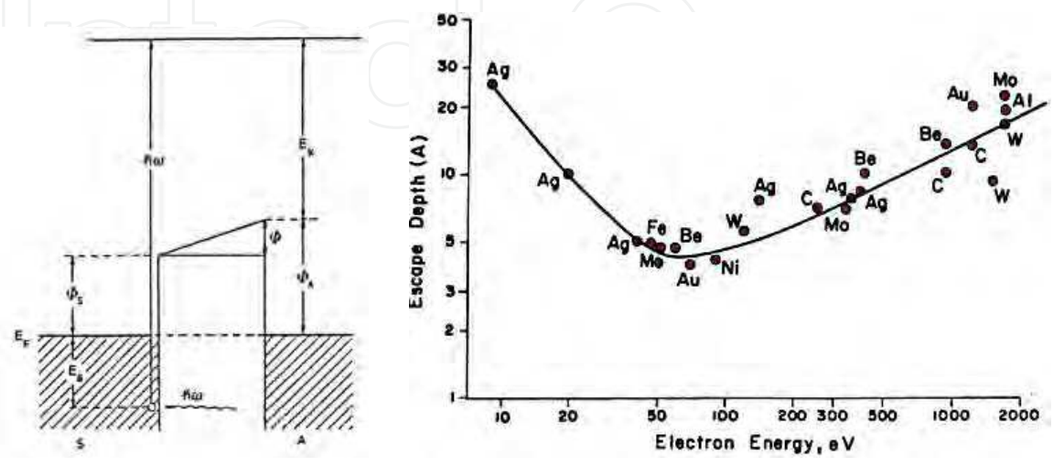

Fig. 5. Left: Level diagram of PES process in a metal. S indicates the sample, A the electron analyzer, E_F the common Fermi level. Right: Electron inelastic mean free path in different materials as a function of their kinetic energy.

Even if the photons penetrate into a solid for several μm, photoemission is a surface sensitive technique. The sampling depth in the photoemission process is determined by the mean free path of the photoelectrons in the solid. This quantity follows the so-called universal curve Shown in Fig. 5 right, and it changes as a function of the electron kinetic energy from about 4Å to about 50Å (Weber, NIST database).

Detecting electrons, XPS must be carried out in Ultra High Vacuum (UHV) conditions. The intensities of the photoemission structures reflect the density of states and depend furthermore on the cross sections of the photoemission processes involving electrons of different energy levels.

XPS sources in campus are normally anode emission of Al Kalpha (1486.6eV) or Mg Kalpha (1253.6eV); synchrotron radiation provide photon energies from approximately 10 eV up to the soft-X ray and hard X ray region. The binding energies of the peaks are characteristic of each element.

A measured XPS spectrum of Au(111) sample is shown in Figure 6a. It is characterized by sharp peaks, superimposed to a mostly featureless background, which exhibits a huge peak (not shown) in the low kinetic energy region (≈5-10eV). This background is ascribed to the almost continuum distribution of the secondary electrons which are produced after inelastic scattering within the solid, thus having lost memory of their primary energy. The excitation of most core levels requires at least soft X-rays, which explains the more usual acronym of the technique. Because of the discreteness of the core levels energies, each core level distribution is a fingerprint of a specific chemical element, thereby making XPS an atom-specific technique.

The peak areas can be used (with appropriate sensitivity factors) to determine the composition of the materials surface. The width of a photoemission core level depends on many different factors: mean lifetime of the photo-hole, electronic excitations, phonon coupling, instrumental broadening. A core level binding energy can shift, depending on the chemical bonds and local environment of a specific atomic site. That implies that the shape of each peak and the binding energy can be slightly altered by the chemical state of the emitting atom. Therefore the analysis of the core level lineshape (taken at high resolution, i.e. resolving power $\Delta E/E \sim 10^{-4}$) provides key information on the chemical bond. Thereby the identification of the chemical state of an atom in an unknown solid system is made possible, consistently with the energy resolution and the actual size of the core level shift. XPS is not sensitive to hydrogen or helium, but can detect all other elements.

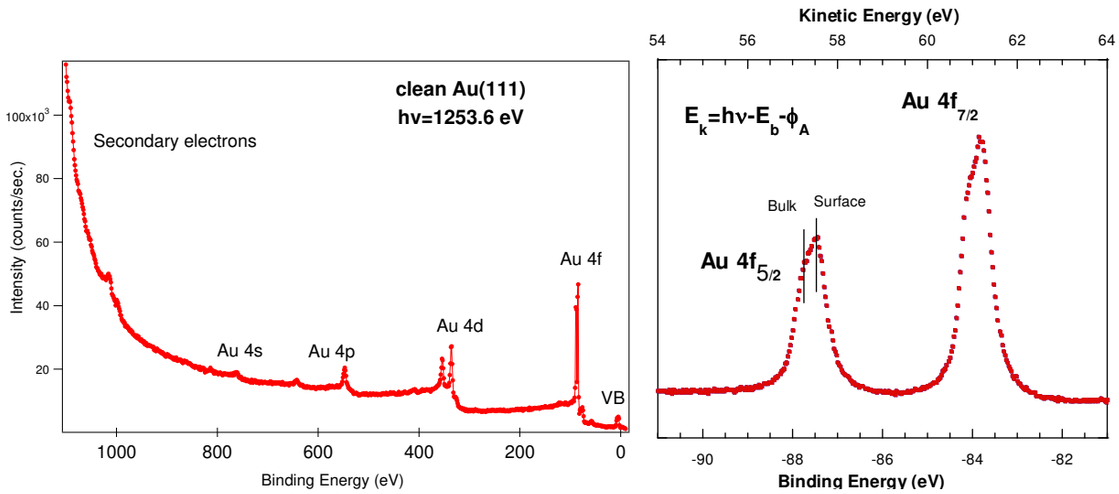

Fig. 6. a) Example of a photoemission spectrum from a Au(111) single crystal (hν=1253.6eV). Core levels and Valence Band emission are indicated; b) high resolution of the Au 4f core level of the Au(111) taken in surface sensitive conditions. The Au 4f emission is a doublet due to the spin orbit splitting of the 4f 7/2 and 4f 5/2. The components ascribed to bulk gold atom and surface atoms are labeled B and S, respectively.

In the photoemission spectra also other structures are visible, typically Auger peaks, shake up losses and correlation satellites due to relaxation processes, i.e. excitation and de-excitation of the system after the creation of the hole left by the photoelectron.

2.3.3 Valence band photoemission and inverse photoemission

The broad structure labeled VB at the low binding energies of the photoemission spectrum in Fig. 6a corresponds to the energy distribution of the valence band states. The typical feature of these shallow states is their delocalized character, compared to the local nature of core levels. They are thus expected to markedly change their distribution in energy as the chemical bonds are changed.

Direct and inverse photoemissions permit a direct measurement of the band structure. With the measurement of *photon* and *Ekin*, PES can determine the occupied state energy. If the

sample is a monocrystal and the electron detector has a finite acceptance angle, one can also use momentum conservation law. Angle Resolved UPS (ARUPS) measures the angular distribution of the photoelectrons as a function of the impinging light angle, i.e. the momentum **k** dependence of the filled electronic states. ARUPS is used to determine the band structure of the material under investigation. As we have seen PES measurement is a mapping of the occupied states of a solid as a function of the binding energy. Once the electron is removed (it is sent above the vacuum level *Evac*), the solid remains in some excited state for a while, with a hole somewhere in the valence states. If the solid used to contain N electrons before the absorption of the photon, it only contains $N - 1$ of them at the end of the process.

UPS can also be used to identify molecular species on surfaces by identifying characteristic the electron energies associated with the bonding orbital of the molecules.

An inverse photoemission experiment is simply the opposite process. This allows a mapping of the empty states as a function of the energy and of the **k**-point of the solid. Here an extra electron is injected with energy *Ekin* into the solid initially in the ground state. It goes down the surface potential barrier φ and arrives in some electronic empty state (eigenstate) of the solid, with emission of a photon of energy $h\nu$. The system of electrons ends in an $N + 1$ particle excited state. As in the direct case, the energy conservation law permits to evaluate the energy of the empty states. Finally, direct and inverse photoemission experiments are the most direct experimental way to measure the band structure of crystals.

A variation of the angle of incidence of the electron beams leads to angle resolved measurements and thus the momentum dependence of the bands. In the isochromat mode, the incident electron energy is ramped and the emitted photons are detected at a fixed energy that is determined by the photon detector. The cross section of the IPS process is five orders of magnitude weaker than photoelectric effect, implying the use of highly efficient photon detectors (Dose, 1985, Luth, 1982).

Figure 7 shows the PES –IPS spectra of a metal (Au(111)) and a thin Ni-octaethyl porphyrin (NiOEP) film. In case of metal surface there is emission at the Fermi level (EF), while in the case of semiconductor there is a gap (transport gap, Et) between the peaks identified as the

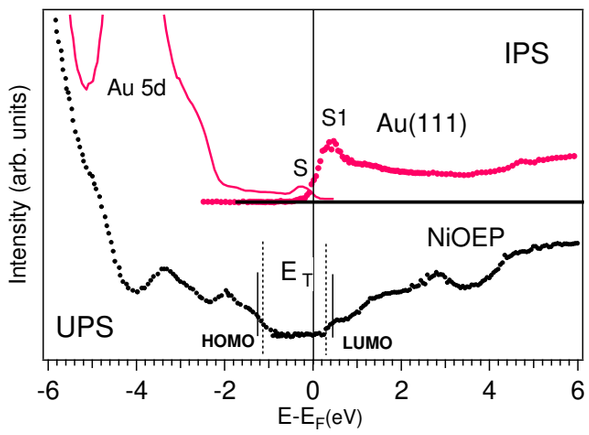

Fig. 7. UPS-IPS spectra of the Au(111) surface (upper red curves) and the multilayer NiOEP (lower black curves). The S and S1 labels indicate the surface filled and empty states, respectively. ET is the transport measured gap.

Highest Occupied Molecular Level (HOMO) and the Lowest Unoccupied Molecular Level (LUMO). In electronic the transport gap, Et, is the energy necessary to create a separated electron–hole pair. The charge injection processes requires promotion of an electron or a hole from the electrodes into one of the charge transport (HOMO or LUMO) states of the organic film. It exceeds the optical gap, Eopt, by 1 eV. (for details see Zahn2006).

2.4 Summary and comparison among the techniques

In section 4 we will discuss our results on organic molecules deposited onto noble metal surfaces, obtained by the described experimental techniques. Table 1 reports the list of typical applications.

Method/Name	Probe/ Signal	Detection limits	Typical applications
Photoemission/X-ray Photoelectron Spectroscopy XPS	Photons/Photoelectrons N-1 final system	0.01-1 at% Surface-bulk sensitive	Surface analysis and composition, Elemental sensitivity, Chemical shifts, stoichiometry
Photoemission/Valence Band UPS	Photons/Photoelectrons N-1 final system	UPS surface sensitive	DOS filled states Energy alignments Transport Gap
Inverse Photoemission/IPS	Elecrtrons/photons Radiative decay N+1 final system	Surface sensitive	DOS empty states Energy alignments Transport Gap
Near edge X ray Absorption Fine structure/NEXAFS	Photons/hole recombination Transitions form core to empty states, N-1 final system	Surface sensitive for adsorbates	Structure Molecular orientation TOGETHER with elemental local density of empty states.
Low Energy Electron Diffraction	Elastic back scattering of low energy electrons	Sub- single monolayer	Surface structure adsorbate structure. Long range order
Surface XRD	Elastic scattering of Hard X-ray photons	From submonolayer to bulk, depending on the incidence X-ray angle and experimental geometry	Atomic structure of surface and interfaces atoms and adsorbates Long range order
Scanning microscopy / STM	Tunneling current	Atomic resolution in UHV	Topography of the surface
Scanning microscopy / STS	**Tunneling current versus bias voltage**	Atomic resolution in UHV	Local Density Of States, absorption gap with atomic resolution

Table 1. Research methods and the typical applications to measure surfaces composition, electronic properties and structures.

3. Main topics of surfaces of noble metal surfaces

Flat surfaces of single crystal samples correspond to a single Miller Index plane and, as we have seen, each individual surface has a well-defined atomic structure. Low index Miller flat surfaces (Ashcroft & Mermin 1976) are used in most surface science investigations. Depending upon how a single crystal is cleaved or cut, flat surfaces of macroscopic dimensions are obtained. As many of the technologically most important metals, noble metals exhibit a face centered cubic (*fcc*) structure. The single crystal surfaces (100), (110) and (111) represent the most frequently studied surface planes of the fcc system (BALSAC web site) - however, they are also the most commonly occurring surfaces on such metals. The knowledge gained from studies on this limited selection of surfaces contributes in propagating the development of our understanding of the surface chemistry of these metals.

By splitting the metal crystal along a specific crystallographic plane, the number of nearest neighbour atoms (coordination number, CN[1]) is reduced. This implies that the energy of the surface atoms is higher than that of an atom inside the bulk. These bulk terminated surfaces rearrange the atoms in order to minimize the surface energy. This produces either relaxation, i.e. vertical rearrangement of surface layers (as for example in fcc (111) surfaces), or reconstruction namely the lateral rearrangement of surface atoms (as in fcc (110)). The minimization of the free energy has the tendency to reduce the surface area, altering the geometry of the surface atoms. In particular relaxation takes place because the surface has a high surface tension and the electrons near the surface tend to smooth their surface electronic charge.

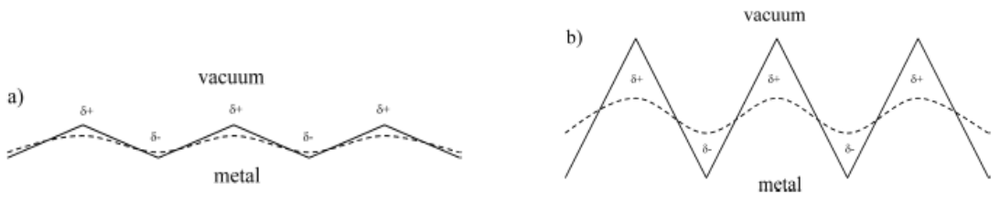

Fig. 8. Illustrations of the Smoluchowski smoothing model due to the redistribution of the charge density at the surface when the density relaxes. a) smooth, closely packed, and b) corrugated loosely packed surface. The lines are related to the contour of the electron density at the surfaces. The dashed lines show the contours after the redistribution of the electron charge density.

The electronic structure of noble metals is due to the simultaneous presence of s and d states in the valence band. The s electrons are essentially free and localized at the Fermi level, while the d states are spatially localized and yield to complex hybridization both in the bulk and at the metal surface. This complexity defines the electronic properties of the surface: the work functions, the surface energies, the reconstructions and the reactivities under molecular absorption. One of the physical observables more used to evaluate the electronic

[1] The Coordination Number of atoms in the bulk of the *fcc* structure is 12. To calculate the CN of a surface we should subtract to the bulk CN (12) those atoms which have been removed from above in forming the surface plane.

properties of surfaces and interfaces is the work function, (Figure 5 left, section 2.3.2) i.e. the energy that is necessary to promote an electron from the Fermi level to the vacuum. The work function (WF) depends on the element and on the structure of the surface. The interplay between the ionic potential (made by the atomic structure) and the electronic charge (filled electron valence states) determines the macroscopic properties of the surface and has strong relevance on technologic applications.

Accurate work functions have now been measured in ultrahigh vacuum for most common metals in various crystallographic orientations. The dependence of the WF on the surface orientation (WF anisotropy) in noble metals has an increasing trend from (110)→(100)→(111). For WF anisotropy the simpler model is the Smoluchowski (Figure 8). This effect (Smoluchowski,1941) consists in the redistribution of the electron cloud on a metal surface with a strong corrugation. Consider a closed packed and an "open" surface of some material. On the open surface we find the Smoluchowski effect of charge smoothing. This smoothing leads to a dipole moment which opposes the dipole created by the flow-out of the electrons. Hence, the work function of a closed packed surface will be higher than that of an open surface. The closed packed (111) surface has the highest workfunction.

Recently (Fall2000, Singh-Miller 2009) ab initio calculations by more accurate microscopic models improved the comprehension of the interrelation between structure and electron density at surfaces.

Theoretical simulations provide trends on the main surface properties. The literature, even recent, is quite rich. For example the evaluation of defect formation, surface relaxation, adhesion at surface, surface energy have been performed for surface atomic scale by effective medium theory (Stoltze 1994) and density functional theory (Vitos et al., 1998, Singh-Miller et al. 2009). Experimental values and example of theoretical results are reported in table 2.

The low values of Adatom/vacancy formation of the Au low Miller index surfaces (Table 2) reflect the high mobility of Gold surfaces (surface energy, E_{ad}/Vacancy) for which it is relatively easy to induce structural changes. The most stable surfaces present high surface atom density and surface atoms with high coordination number fcc(111)>fcc(100)>fcc(110).

The physical definition of a noble metal requires that the d-bands of the electronic structure are filled. Taking this into account, only copper, silver and gold are noble metals, as all d-like band are filled and don't cross the Fermi level (EF, fig. 5) that is the highest energy level that is occupied by the electrons in the metal. Other catalytically important precious metals (Pt, Rh, Pd) shows a more complicated configuration: for platinum two d-bands cross the Fermi level, changing its chemical behaviour. Note the reduced 6s-5d separation of ≈ 2 eV in gold as compared to ≈ 3.5 eV for the 5s-4d separation in the silver atom. This suggests the higher reactivity of silver.

The structure has a strong influence on the electronic properties and reactivity of the surfaces. Reactivity variations to different gases and deposited molecules on the surface even of the same metal are commonly measured. Reactivity strongly depends on the electronic properties, and hence on the crystallographic orientation of the surface (Hammer, 2006). The Hammer-Nørskov d-band model correlates changes in the energy center of the valence d-band density of states at the surface sites with their ability to form chemisorption bonds. A reactivity change is characterized as an electronic structure effect. In this way the

model can explain the reactivity change from flat Au surfaces, over Au thin films to Au edges. The different reactivity can easily be seen while preparing clean metal surfaces in ultra high vacuum; surfaces of "physical defined" noble metals (e.g., gold) are easy to clean and stay clean for a long time, while those of platinum or palladium, for example, are covered by carbon monoxide very quickly.

Surface	a_0 /Å	Area unit cell a 2D /Å^2	2DBrillouin zone	Surface density/ (at/cm2)/ CN	WF (eV) Fall,2000/ Singh-Miller 2009	Surface Energy γ (J/m^2) Vitos 98	Theory Adatom/ vacancy Energy (eV) Stoltze 1994
Cu(111)	3,61	$\sqrt{3}/4a_0^2$	hexagonal	$1.78 \cdot 10^{15}$ /6	4.95	1.79	1.329
Cu(100)		$1/2a_0^2$	Square	$1.09 \cdot 10^{15}$ /4	4.6		0.984
Cu(110)		$\sqrt{2}/2a_0^2$	Rectangular P	$1.53 \cdot 10^{15}$ /2	4.45		0.466
Ag(111)	4.09	$\sqrt{3}/4a_0^2$	hexagonal	$1.38 \cdot 10^{15}$ /6	4.74	1.246	1.027
Ag(100)		$1/2a_0^2$	Square	$8.45\ 10^{14}$ /4			0.694
Ag(110)		$\sqrt{2}/2a^2$	Rectangular P	$1.20 \cdot 10^{15}$ /2			0.327
Ag poly					4.26		
Au(111)	4.08	$\sqrt{3}/4a_0^2$	hexagonal	$1.39 \cdot 10^{15}$ /6	5.3	1.5	1.009
Au(100)		$1/2a_0^2$	Square	$8.45\ 10^{14}$ /4	5.22		0.556
Au(110)		$\sqrt{2}/2a_0^2$	Rectangular P	$1.20 \cdot 10^{15}$ /2	5.2		0.273
Au poly	4.08				5.1		
Pt(111)	3.92	$\sqrt{3}/4a_0^2$	hexagonal	$1.51 \cdot 10^{15}$ /6	6.08	2.49	1.429
Pt(100)		$1/2a_0^2$	Square	$9.20\ 10^{14}$ /4	5.82		0.818
Pt(110)		$\sqrt{2}/2a_0^2$	Rectangular P	$1.30 \cdot 10^{15}$ /2	5.35		0.370

Table 2. Comparisons of low index metals surfaces of Cu, Ag, Au and Pt: structural symmetries, surface density, experimental work function, calculated surface energies and vacancy-adatom energy formations.

3.1 Two extremes: Comparison between (111) and (110) surfaces

In case of the [111] planes noble metal (Cu, Ag, Au and Pt) have a close packed structure, while the surfaces having [110] orientation are more "open" and a (2x1) reconstruction can take place at RT.

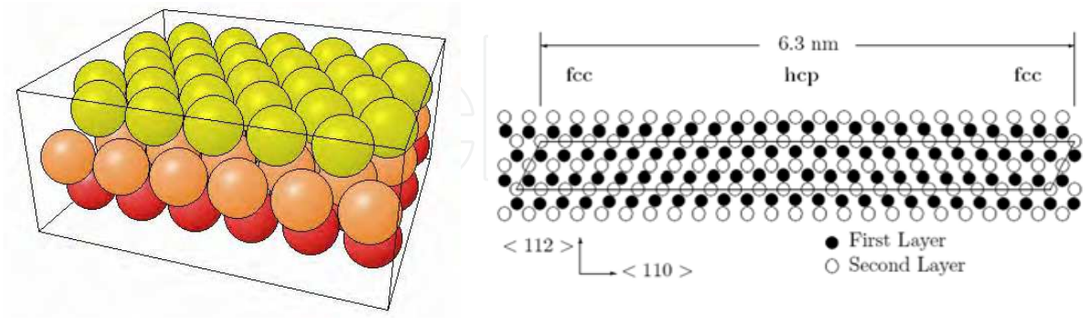

Fig. 9. Left: Structure bulk terminated fcc (111) [2]. Right: side view of the Au(111) herringbone reconstruction

The (111) surface is obtained by cutting the fcc metal in such a way that the surface plane intersects the x-, y- and z- axes at the same value - this exposes a surface with an atomic arrangement of 3-fold (apparently 6-fold, hexagonal) symmetry. This layer of surface atoms actually corresponds to one of the close-packed layers on which the fcc structure is based. This is the most efficient way of packing atoms within a single layer.

In a fcc (111) surface all surface atoms are equivalent and have a relatively high CN and the surface is almost smooth at the atomic scale.

The surface offers the following adsorption sites: On-top sites, Bridging sites, between two atoms, Hollow sites, between three atoms.

The effect of surface formation induces relaxation of the topmost metal layer. For example the clean Pt(111) surface does not show any reconstruction, however a S-XRD analysis of its CTRs (see section 2.1) shows that the surface top layer is slightly relaxed with respect to the nominal bulk termination and their fitting allows to determine an expansion of 4.5 ± 0.5 pm *(+2.0%)* with respect to the ideal bulk termination (Felici&Pedio 2009). Au(111) clean surface shows a Au (111) 22 √3 "herringbone" reconstructed surface (van Hove 1881, Sandy 1991), that involves a great number of surface atoms (Fig. 9 left , Herringbone side view, STM image Fig. 1 right).

The (110) surface is obtained by cutting the fcc unit cell in a manner that intersects the x and y axes but not the z-axis - this exposes a surface with an atomic arrangement of 2-fold symmetry i.e. a rectangular symmetry of the surface layer atoms. In one direction (along the rows) the atoms are in contact i.e. the distance between atoms is equal to twice the metallic(atomic) radius, but in the orthogonal direction there is a substantial gap between

[2] The pictures of figure 10 left and 11 left have been made from NIST SSD output and processed with BALSAC by K. Hermann. http://www.fhi-berlin.mpg.de/~hermann/Balsac/SSDpictures.html SSD is the NIST Standard Reference Database no. 42 by P. R. Watson, M. A. Van Hove, and K. Hermann

the rows. This means that the atoms in the underlying second layer are also, to some extent, exposed at the surface. Normally the bulk terminated (110) plane is energetically not favourable. The (110) surfaces of Ag and Au metals are characterized by the strong surface diffusion anisotropy energies. Typically this surface can be unstable and shows reconstructions ranging from the 1x2 to the 1x5 unit cell.

The clean Au(110) presents the missing row 1x2 reconstruction, while Cu(110) remains unreconstructed (Africh, 2010) as shown in Figure 10.

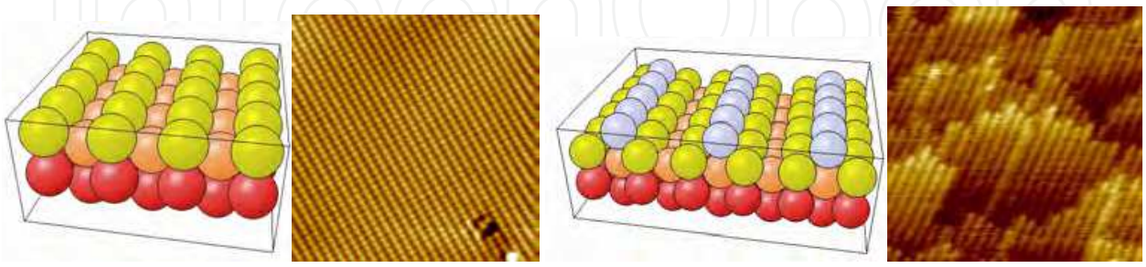

a) Cu(110)b) Au(110) (2x1) Missing row

Fig. 10. a) bulk terminated fcc (110) picture and STM image of Cu(110) surface (C. Africh). B) (110) missing row 2x1 reconstruction picture and topographical image of Au(110) 2x1 reconstruction ref. http://www.redespm. org.br/grupo10.html

The (110) substrates have higher mobility and reactivity. They offer a wide variety of possible adsorption sites, including : On-top sites, Short bridging sites between two atoms in a single row, Long bridging sites between two atoms in adjacent rows. Moreover higher coordination sites are possible (in the troughs that are facets with (111) orientation). The Au(110)-(1×2) surface shows an order-disorder transition with critical temperatures, Tc, between 650 K and 695 K depending on finite-size effects (Clark, 1986).

A large number of experimental and theoretical works have been envisaged to single out the basic aspects of molecules interacting with noble metal. In particular, the Au(111) surface is widely used as support of SAM providing an almost uniform reserve of electron charge. Differently from the (111) case, in a (110) 2x1 reconstructed fcc surface, the surface is atomically rough, and highly anisotropic. The surface atoms on a more open ("rougher") surface have a lower CN - this has important implications when it comes to the chemical reactivity of surfaces, as we discuss in the next section.

4. Survey of ordered molecular layers: From weak interaction to anchoring

Organic molecules can provide complex functionalities at a metal surface. The engineering of the functionalities of organic-inorganic interfaces has important technological applications, as cathalysis, sensors, optoelectronics, molecular spintronics, photovoltaic and so on. The development in these fields implies a deep understanding of the bonding and the lateral interactions that govern the organization of the molecular thin films and ultimately the design for the optimization of their functionalities. In order to accomplish this goal a rigorous surface science approach is necessary: dosing of known molecular fluxes on defined surfaces under ultra high vacuum conditions and fine characterization of these systems, including sophisticated data analysis, theoretical modelling and simulation.

The molecular ordening onto surfaces strongly depends on the delicate balance of the molecule-molecule and molecule-surface interactions (see discussions in ref. Rosei et al. 2003). This is reflected in the complexity of the phase diagrams of these systems. Small differences in the properties of the noble metal substrates (discussed previously) can lead to marked differences in the molecular deposited layers.

Depending on their structure the molecular semiconductor ordered films have important properties for microelectronics: integrability with inorganic semiconductor, low cost, large area bulk processing, tailoring for specific electronic and optical properties, systems more tolerant of defects (no electronically active), no dangling bonds that leads to great flexibility on the choice of substrates, charged carrier mobility increases with increasing pz-pz orbital, anisottropic mobility (for axample Pentacene μ*~1 cm²/Vs direction in-plane,* μ *~10⁻⁴ cm²/Vs stacking).*

The disadvantages concern mainly the fact that a high degree of molecular ordering is necessary, to avoid the problems related to low carrier mobility.

The growth procedures are relevant in the bond, ordening and structure of the monolayer of organic semiconductors. All the cases discussed in the following are related to vapor deposition in UHV conditions.

We compare different single organic layers deposited onto ordered noble metal surfaces. The interest and the strong effort in the characterization of the first MONOLAYER[3] of organic molecules on single crystal surfaces adsorption is due to the general accepted result that structural and chemical properties of the monolayer are keys for controlled multilayer growth. The nucleation, growth, structure and interaction molecules strongly depend on the substrate nature and on the particular experimental protocol used during the deposition. The geometry of the first organic layer is exploited to drive the orientation of the next growing layers. From the electronic point of view, the first layer acts as a buffer layer, enabling the following layers to be exploited for the intrinsic electronic properties of the free molecule. Case studies of molecules that differ in size, symmetry and morphology, deposited on different low index noble metal substrates are here presented, on the basis of structural and electronic properties determined by the above techniques (section 2). Figure 11 shows the structural formulae of the molecules discussed in the following. Due to the extension of the literature on SAM deposited onto noble metal surfaces, the list of systems treated in this chapter cannot be complete. We focus our attention on our results obtained on ordered molecular layers mainly deposited onto Au(111) and Au(110) substrates, considering gold as the prototypical noble metals. Other specific systems involving other metal surfaces will be taken into account and discussed.

The large dimension of these molecules (scale 10 Å) with respect to the unit cell of metal surfaces (Table 2), implies that the local molecule-substrate interaction involves several unit cells of the substrate. The properties of these low dimensional systems depend, for example, on the nature of the chemical bond (ionic *versus* covalent *versus* Van der Waals), on the partial filling of the lowest unoccupied molecular orbital (LUMO) as a result of a charge

[3] For example 1 ML on Au(111) is defined as the packing density compared to the Au(111) plane, $1.39 \cdot 10^{15}$ atoms/cm², which is equivalent to an effective thickness of 2.35 A ˚ at the density of bulk gold.

transfer from the substrate and/or from dopant atoms (influenced by the substrate work function, the molecule-substrate interaction and possible screening effects), on the geometry of the molecular film which depends on the substrate surface chosen and on the thermal history of the film) , on possible adlayer-induced substrate reconstruction and on defects. In the next section we will describe the research methods with some detail.

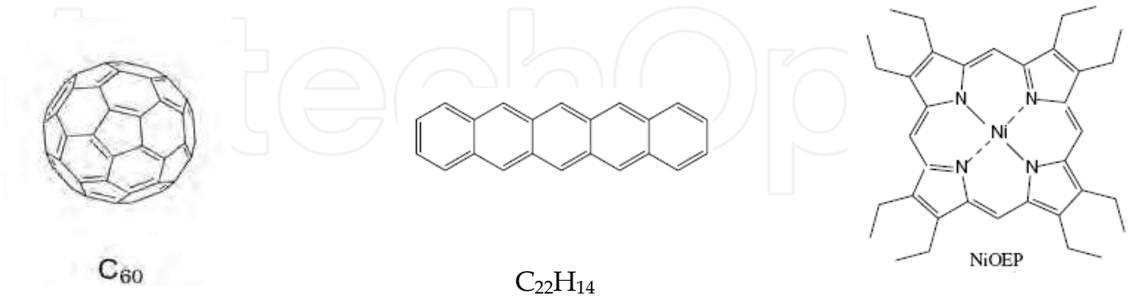

C_{60} $C_{22}H_{14}$

Fig. 11. Structures of different molecules. Left: Fullerene C_{60}, Center: Pentacene $C_{22}H_{14}$, Right: Ni Octaethylporphyrin NiOEP.

4.1 C_{60} on noble metals

Fullerenes (C_{60}) can be considered as model systems of large molecules. This kind of soccer-ball shaped molecule with its three dimensional character along with the strong modulation of the valence charge distribution over the molecular cage. This unique electronic structure leads to several possible interaction mechanisms with the host surface. The geometrical constraints imposed by the three dimensional cage allow only a few carbon atoms per molecule to be in contact with the substrate. The distribution of electronic charge (interface region) and the electronic properties of the first C_{60} ML can be tuned. When deposited on a single crystal surface, fullerene molecules are proving useful to encapsulate surface reconstructions and/or are functioning as templates for the formation of novel structures. They are widely used to create complex architectures on surfaces for their stability, electronic properties (doping), functionalization, and capability of forming reconstructed surfaces (Rudolf 1996 as cited in Gavioli &Cepek, 2008).

Monolayer (ML) and sub-monolayer films based on fullerene molecules deposited on top of metal or semiconductor surfaces, therefore, form a class of systems that could exhibit a wide range of physical behaviours. An increasing number of works is aimed at studying the interaction of single layers of C_{60} with nobel metal surfaces. Due to its large work function (7.6 eV) and electron affinity (2.7 eV), C_{60} has the propensity to accept electrons from many metallic surfaces. However, charge transfer from the metallic substrate to C_{60} is not always observed and the character of the interaction depends mainly on the metal, almost independently of its work function. Thin films of C_{60} adsorbed on crystalline substrates usually tend to form hexagonal or quasi-hexagonal ordered structures with a large variety of the substrate-adsorbate interactions, ranging from covalent to ionic character. An important issue is the investigation of the consequences of the C_{60} adsorption on the underlying substrate structure. According Maxwell et al. (Maxwell 1994) the bonding interaction of C_{60} in direct contact with a metal surface can be divided in three categories:

strong predominantly covalent bonding, intermediate predominantly covalent bonding and intermediate predominantly ionic bonding. Strong predominantly covalent bonding has been observed for a single layer of C_{60} on Ni(110), Pt(111), Rh(111) and Ta(110) where the strength of the interaction is able to catalyze the fullerene cage decomposition prior to the desorption of the monolayer. Interaction of intermediate strength with bonds of mixed ionic character has been observed for the C_{60} monolayer on Au(110), Au(111), Ag(110), Ag(111) and polycrystalline Ag Cu(110) and Cu(111),. Charge transfer has also been observed for C_{60} monolayers deposited on polycrystalline Au and Cu samples, but the stability of the C_{60} monolayer and the strength of the interaction onto these surfaces was not investigated in detail. The trend of these bond strengths reflects the Hammer- Nørskov model (par. 3).

A particular case has been observed on Ag(100). By using the appropriate sample preparation conditions, this system shows the reversible opening of a gap at the Fermi level at temperatures 25 ≤ T< 300K (see Fig. 12), whose origin is still under debate (Cepek et al. 2001, Goldoni et al., 1998).

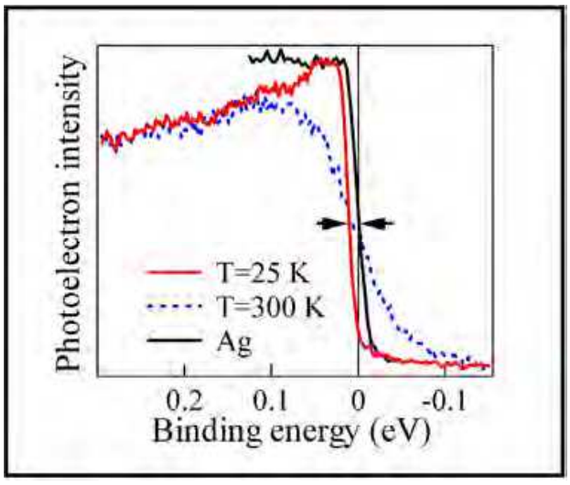

Fig. 12. Fermi Level photoemission spectra of the C_{60}/Ag(100) system at varying the temperature.

The C_{60} layer may not present long-range order, but in any case the quasi-hexagonal geometry is locally preserved. The C_{60} molecules adsorbed on Ag(100) follow this general trend. The growth mode and morphology of the C_{60} molecules adsorbed on Ag(100) at room temperature (RT) or above has been widely studied (Goldoni, 1998, Giudice,1998), Cepek,2000a), Lu, 2003). It has been observed that the C_{60} molecules form a strong bond on the Ag(100) surface at any growing temperature investigated (for STM, ranging from 100K to ≈670K). When deposited at room temperature or below, and by using an evaporation rate of ≈0.2ML/min.), the growth mode is not layer by layer, but the second layer start to grow before the first is completed (Fig. 13, a, b) (Cepek, 2000 a). When the C_{60} molecules are deposited at a temperature higher than the C_{60} sublimation temperature, or by annealing a C_{60} multilayer film, only one single layer of molecules are left on the surface. When the annealing or growing temperature is higher that ≈600K the molecules form a well ordered overlayer, characterized by long range order and by a sharp quasi-hexagonal LEED pattern, where the C_{60} - C_{60} distance is ≈10.4Å (see Fig. 13 c).

The most direct experimental technique, giving detailed information regarding interaction between the fullerene molecules and the substrate, is PES valence band (VB). Fig. 14 left compares the VB spectrum of the ordered monolayer with the clean substrate and the C_{60} multilayer. The spectra were measured at room temperature (RT) (Cepek, 2000 a). The C_{60} multilayer spectrum is the typical molecular-like spectrum of this compound. The five-fold degenerate highest occupied molecular orbital (HOMO) derived band lies at energy of ≈2.2eV, while the HOMO-1 derived band has energy of ≈3.6eV. The clean Ag(100) spectrum does not show any features in the HOMO and HOMO-1 energy range, so all the structures observed in the ML spectrum in this region are only due to the C_{60} adsorbed. We note that the ML spectrum shows an extra emission at the Fermi level compared to the multilayer spectrum, indicating a metallic behaviour. We want to remark that this extra emission cannot be due to the metallic Ag substrate, if the strong attenuation by the C_{60} layer is considered. So it results that the presence of the peak at the Fermi level is the typical fingerprint of a partially filling of the C_{60} lowest unoccupied molecular orbital (LUMO) derived band and it means that charge transfer from the Ag substrate to the C_{60} molecules takes place. By K doping, it has have found that the molecules adsorbed on the monolayer are in a charge state ≈-2 (Cepek, 2000 b)). Finally we want to note that the bond is activated by temperature.

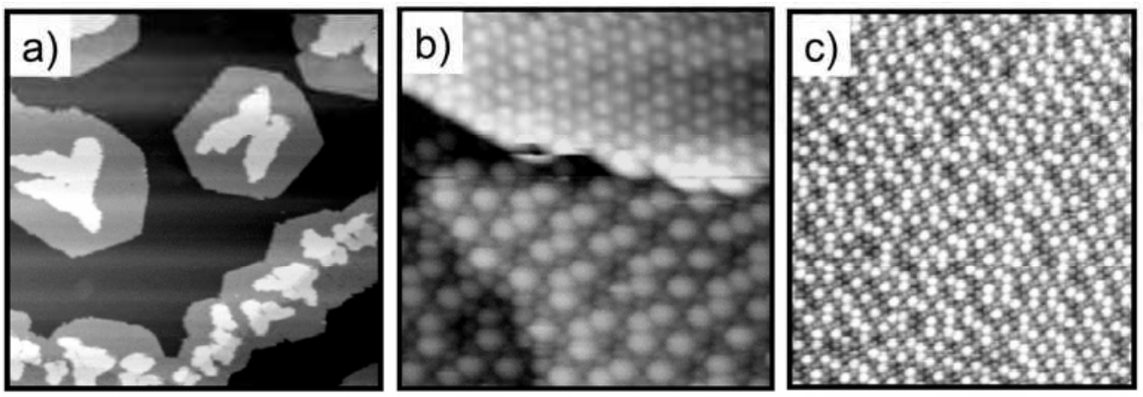

(Cepek et al., 2000 a)

Fig. 13. STM images of different C_{60} coverages deposited on Ag(100). See text for discussion.

Fig. 14, right shows the VB photoemission spectra of 0.7 ML of C_{60} adsorbed on Ag(001) at 150 K and subsequently annealed to different temperatures (RT and 600 K for ≈ 5 minutes, compared to a thick C_{60} multilayer (Cepek, 2000 a). The 150 K spectrum has been measured at 150 K, all the others at RT. The deposition of the same quantity of C_{60} molecules at RT produces a photoemission spectrum (not shown) identical to that of the 150 K deposited film annealed at RT. The same is true for the spectrum of a 600K deposited or annealed film.

Also in this case, the adsorption of C_{60} induces an increase of the photoemission intensity at the FL with respect to the clean surface thereby indicating that in all samples the bond is characterized by charge transfer from silver atoms to C_{60} molecules. The 150 K and RT VB photoemission spectra show that the HOMO and HOMO-1 derived bands consist of two components: one centered at the same BE of the multilayer spectrum, the other at the BE of one ordered C_{60} ML. This, combined with the STM images of Fig. 13 a, allows us to attribute

the former component to C_{60} cages in the second layer and the latter to C_{60} molecules in direct contact with the substrate. Data fittings (continuous line of Fig. 14, right. See Cepek2000 a, b for more detail) confirms this hypothesis, showing that the percent of the molecules of the second layer is $x \cong 24\%$ for the 150K spectrum and $x \cong 20\%$ for the RT spectrum. The very good agreement of these results with the value of 17% obtained by STM, confirms that the molecules in direct contact with the substrate present the same bond at 150 K, RT, and 600 K while the second layer molecules do not interact with the substrate, as already observed for different systems (Cepek et al., 2000a). Taking into account that core level spectra indicate that no C_{60} molecules desorbs passing from 150 K to RT, this indicates that the increased thermal energy enables a fraction of the second layer molecules to descend the step edge and to incorporate in the first layer islands. From a careful inspection of the fittings in Fig. 14 right) (continuous line), one can notice that the 150 K deposited film spectrum is slightly sharper than the simulation result. This is due to the specific phonon broadening of the experimental data (measured at 150 K), which is lower than that used in the simulation, performed using spectra measured at RT. However it presents also lower photoemission intensity at the Fermi level with respect to the simulation, which can not be due to the different temperatures and may indicate a lower C_{60} charge state, or a higher disorder. In spite of these minor differences, passing from 150 K to RT, there is no evidence for the appearance of two different electronic states corresponding to the two different kinds of molecules (bright and dim) observed in STM images, which may be easily explained with the occurrence of the two molecular orientation revealed by the high resolution STM images (Lu, 2003) and by XPD.

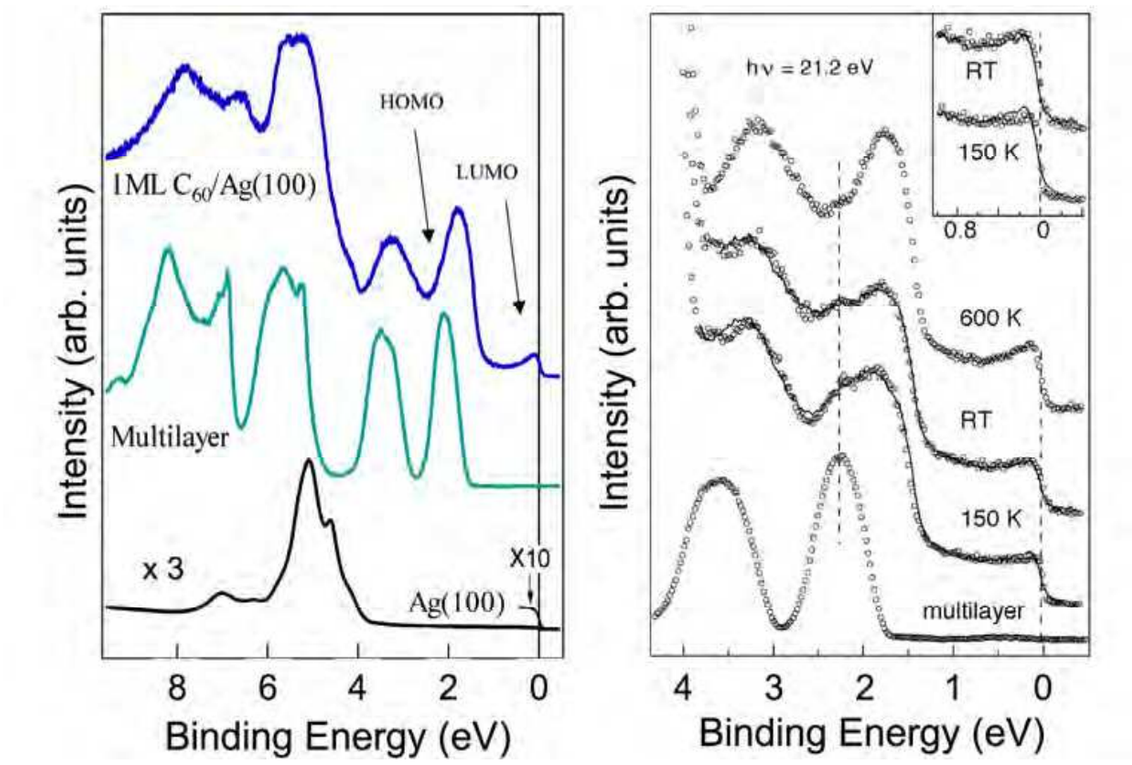

Fig. 14. Left: Valence Band spectra of C_{60} deposited onto Ag(100) . Clean Ag(100) and C_{60} Multilayer are compared. Right: Valence Band spectra for different Temperatures. See text for details.

We discuss two cases systems: the "covalent" C_{60}/Pt(111) (Felici, 2005) with the partially "ionic" C_{60}/Au(110) (Pedio et al., 2000, Hinterstein et el., 2008) systems.

Fig. 15 shows the phase diagram of the C_{60} deposited onto Pt(111) surface. The C_{60} deposited on Pt(111) at room temperature weakly interacts with the substrate atoms and molecular features measured by electron spectroscopies are similar in intensity and energy separation to the isolated molecule or to C_{60} multilayer. After annealing the fullerene bond with Pt(111) substrate become strongly covalent. The deposition of one monolayer of C_{60} on the Pt(111) surface at T < 580°C leads to an ordered double domain hexagonal reconstruction, that is present also for coverages exceeding 1 ML (Pedio et al., 1999, Felici et al., 2005].

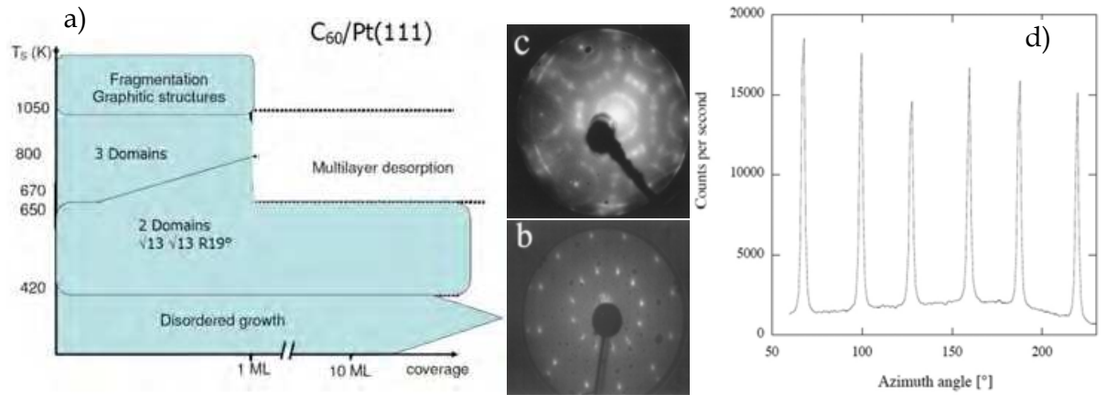

Fig. 15. a) Phase diagram of the C_{60}/Pt(111) systems obtained with C_{60} flux of 0.05 ML/min and slow temperature variations (1 K/min). The peaks belong to the two hexagonal domains separated of 27.8°, b) LEED pattern of the single layer of √13 √ 13*R*13.9° , c) LEED pattern of the hexagonal 3-domain reconstruction. d) Azimuthal scan of the x-ray scattered intensity for an exchanged vector modulus corresponding to the first order of the √13 √ 13*R*13.9° reconstruction.

The long range molecular ordening formation is a kinetically controlled process. The double hexagonal pattern was observed even for 1 ML adsorbed at 100 K and annealed above 770 K (Cepek et al., 1996). When the sample is heated above 800 K or if less than a complete monolayer is adsorbed at T>670 K, a third domain becomes visible in the LEED pattern.

About 10 MLs of C_{60} were deposited at room temperature. Then the system was slowly annealed while monitoring with the x-rays the appearance of the √13 √ 13*R*13.9° reconstruction. At about 420 K sharps peaks corresponding to this reconstruction appear. This temperature is much lower than the multilayer desorption of the fullerenes and, in fact, x-ray reflectivity scans show the presence of a well ordered C_{60} multilayer. In Fig.15 d) we show an azimuthal plot of the intensity of the fist order reconstruction. The two P6 domains separated of 27.8° with a practical equal intensity are clearly observable. Further annealing at 650 K removes the multilayer and leaves only one layer bonded to the surface. The analysis of the CTRs provides the following information: a) the vertical expansion of the topmost substrate layer reduces to 1.1 +/- 0.4 pm, b) the increase in surface roughness is compatible with the presence of one vacancy per reconstruction unit cell in the substrate surface.

From the x-ray diffraction analysis this vacancy helps enormously the structural solution of the system. In our case the vacancy can be considered as a heavy atom with a negative number of electrons and the Patterson must then be interpreted by looking at the negative peaks (Fig.16). The dashed rhombus in the figure shows the surface unit cell of the Pt(111) substrate while the large continuous line rhombus is the surface unit cell of the √13 √13*R*13.9° reconstruction. The dashed contour lines represent the negative values of the map and the deepest minima are localized around the vacancies and at the Pt surface atom positions. A fitting of the data, assuming only 13 structural parameters, leads to a very simple solution of this complicated system. The surface Pt atoms displace slightly from their bulk terminated positions while the C_{60} lies on top of the vacancies pointing to the substrate surface with one of its hexagonal surfaces. The fullerene enters as much as possible in the vacancy trying to maximize the number of bonds which are formed with the Pt atoms and about 12 Carbon atoms form directs bonds with the Pt substrate. The C_{60} lies with one of its hexagonal faces on top of the vacancies at a height slightly larger than in the case of the Pt substrate. Similar results have been also observed in the case of the C_{60} adsorbed onto the Ag(111) (Li etal. 2009) and the Au(111) surface. Also in these cases the dominant effect is the formation of vacancies at the substrate surface which stabilize the position of the fullerene molecules. In case of Au(111) substrate the number of C-Au bonds is 6, and the herringbone substrate reconstruction is disappeared indicating the release of the stress of the topmost layer, induced by the C_{60} monolayer.

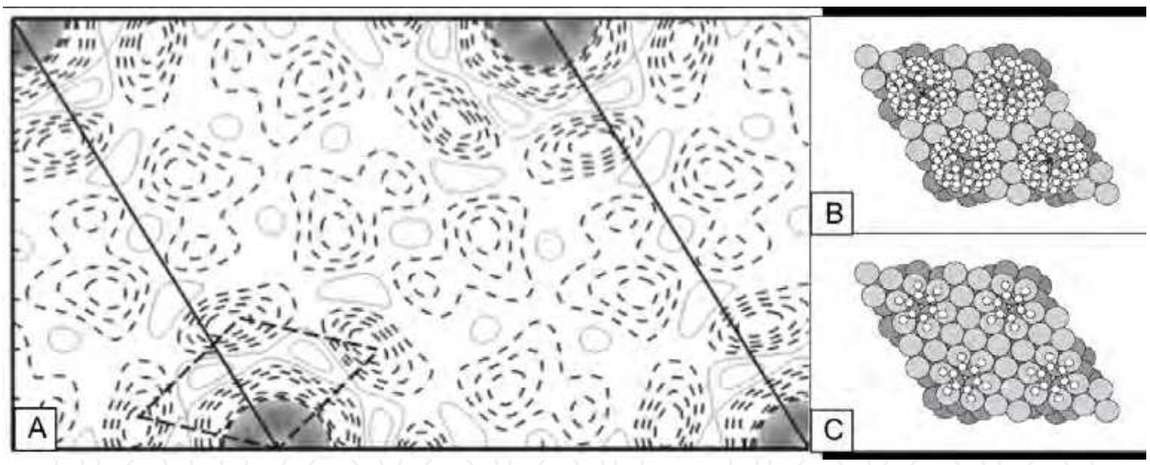

Fig. 16. a) the Patterson map of the √13 √13*R*13.9° reconstruction. Because the pattern is dominated by the signal due to a vacancy in the surface unit cell this map has an inverted sign usual. The negative peaks (dashed lines) correspond to the positions of atoms participating in the reconstruction. The dashed rhombus is the Pt(111) surface unit cell. In (b) we show a top view of the best model fit and in (c) a detail on the C atoms forming bonds with the substrate.

Figure 17 shows the spectroscopy results of C_{60} monolayers deposited onto different noble metal surfaces. On the left the photoemission of the C1s core levels of the ordered monolayers (Maxwell et al 1994, Pedio et al. 1999 private communication) are compared (bottom curve) with that relative to the pristine C_{60}. Note that the bulk C_{60} is a molecular solid tìwith the fullerene that interact by weak, Van der Waals interactions and the spectra are comparable (even though broader) with those obtained on the free molecule in gas

phase. The experimental width in all monolayers is about 1 eV, a value sensibly higher than that of C_{60} pristine. This implies that the C atoms in the single layer have different chemical configurations (C-metal bonds) with respect to the C_{60}. Figure 17 left shows a set of IPES spectra for low coverages of C_{60} deposited on Pt(111) at RT and the single monolayer evolution after annealing at different temperatures. The bottom curves, related to the multilayer and the clean Pt(111), are shown for comparison. The top most spectrum is related to the chemisorbed (6x5) C_{60}/Au(110) that will be discussed in the next section. IPES spectra of the hexagonal phases of a single monolayer are substantially different from the C_{60}-Au(110) where was estimated by electron spectroscopies and an ionic character dominates interaction a charge transfer of 1±1 (see for discussion Hinterstein et al. 2008, Felici et al. 2009) electron. When the surface is annealed a 2-domain structure is formed rather dramatic changes in the spectrum IPES spectrum occur: the LUMO-derived feature appears centered at 0.5 eV and the spectral weight near EF is greatly increased, indicating that there is a redistribution of the empty states. This fact has been interpreted as a strong interaction between the substrate and the C_{60} overlayer when the covalent bond takes place. This result nicely confirms the formation of 12 Pt-C bonds, suggested by the SXRD analysis.

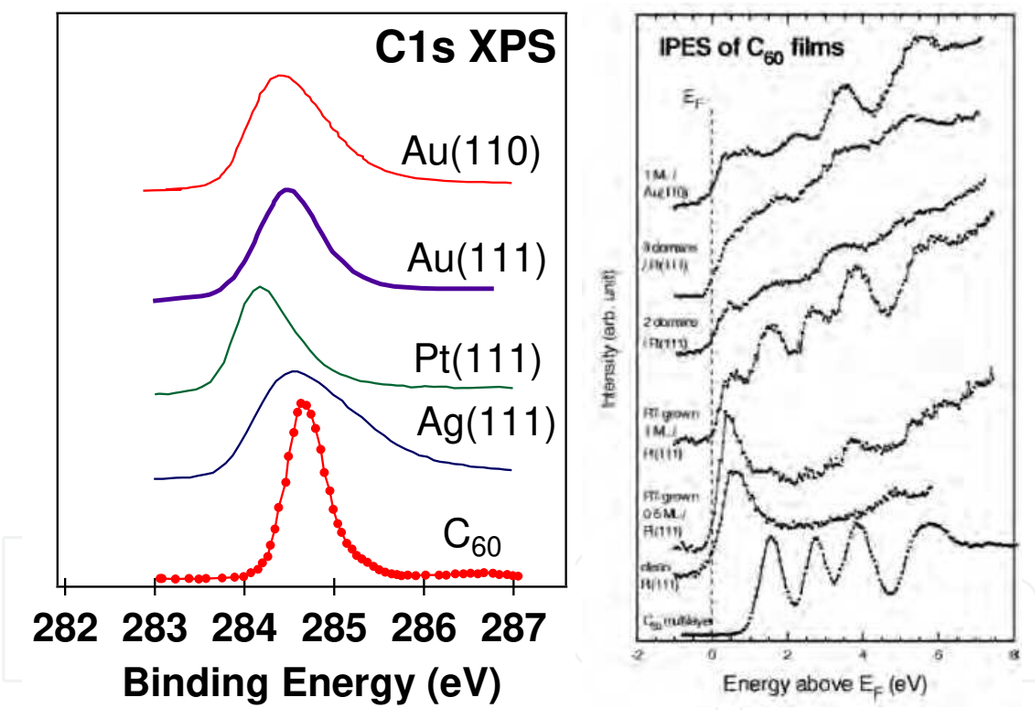

Fig. 17. a) C1s photoemission spectra of C_{60} deposited onto Ag(111), Pt(111), Au(110) and pristine C_{60}. b) Example of IPES spectra taken at normal incidence for different C_{60} overlayers on Pt(111). The spectra for the chemisorbed 1 ML C_{60}/Au(110) (top) and for the multilayer of C_{60} on the same Au(110) (bottom) are plotted for comparison (Pedio1999).

For the two-domain structure on Pt(111), vibrational studies have indicated no evidence for charge transfer. Actually in case of Pt substrate a further annealing of the system leads to a 3-domain structure and to fragmentation of the fullerene. The corresponding LEED pattern shows graphitic rings. Higher T and longer annealing produces changes in the IPES spectra. At this stage it has been suggested that the fragmentation products consist in pentagon-

hexagon groups, still arranged in a pseudo-order related to graphitic-like features in diffraction, as discussed in ref. Pedio 1999.

Upon deposition of 1 ML of C_{60} on Au(110) it is possible to observe by STM a nice hexagonal pattern of the fullerene layer showing alternating brighter and darker lines. The uncovered regions of Au modify their reconstruction from 1x2 to a 1x5 surface cell. This 1x5 reconstruction is in perfect register with the brighter and darker lines in the STM images leading the authors to conclude that this kind of reconstruction was extending under the fullerene layer (Modesti et al. 1996 cited in Pedio et al. 2000). On clean 2x1-Au(110) deposition of few monolayers of C_{60} followed by thermal annealing leads to the formation of large terraces showing a (6x5) reconstruction. The evolution of the IPES spectra of C_{60} deposited on Au(110) for different molecular depositions at room temperature (RT) (Pedio et al. 1995 cited in Pedio et al. 2000) shows, for coverages < 1 ML, that all the molecular structures are broader and their energy separation is different with respect to the multilayer spectrum.

The first structure (LUMO) is practically not detectable and a clearly Fermi level emission is present. As soon as we reach the second layer, the LUMO feature appears clearly, though the peaks are still broader than in the multilayer system. For 1 ML deposition at about 450 °C we observed, in the LEED pattern, a (6x5) superstructure. The energy position of the features in the IPES spectra corresponds to the peaks of the 1ML C_{60} grown at RT, while their intensities resulr much more pronounced. The LUMO emission is confused with the Fermi. The topmost spectrum of Fig. 17 b) shows the 6x5 C_{60}/Au(110). During the formation of the first monolayer, when the system is annealed (either during C_{60} deposition or after) there is a strong deformation of *all* the molecular C_{60} localized states due to a charge transfer from the substrate to the C_{60} indicating a chemisorbed phase. SXRD data confirmed a strong redistribution of the substrate Au atoms induced by the formation of the 6x5 reconstruction after thermal annealing. When analyzed with x-ray diffraction the structure of the interface appeared to be much more complicated. The substrate reconstruction was not a "simple" 1x5 but a complex 6x5 reconstruction with no obvious symmetries. This makes the data analysis an almost impossible task. For solving this system we have applied direct methods which are able to provide hints on the electronic density maps of the surface unit cell (Pedio, 2000).

Starting from the model proposed by the direct methods, we have been able to refine the analysis and obtain a full 3D solution of the system (Hinterstein 2008). The peculiarity of this solution is the proof that fullerene adsorption induces a strong mass transport involving several layers of the substrate. The gold surface modifies itself in order to form a kind of calyx structure where the fullerene molecules fit. Using this proposed structure we have been able to calculate the electronic properties of the interface which can then be compared with the PES data (Fig. 18). The larger contact area between the C_{60} and the metal, resulting from the substrate rearrangement, allows for the formation of strong directional C-Au bonds. The theoretical simulations based on the SXRD model can single out the contributions of HOMO and LUMO of the spectra in PES and IPS (see Fig. 18), and clarify the LUMO contribution and the "ionicity" character of the bond.

Summarizing, in C_{60} deposited on (111) and (110) substrates the formation of directional bonds between C and substrate reconstructed atoms is the important factor of the high

degree of metal surface deformation. These dimples formation is a thermally activated process that produce an anchoring of the molecule. The molecular states are results strongly hybridised.

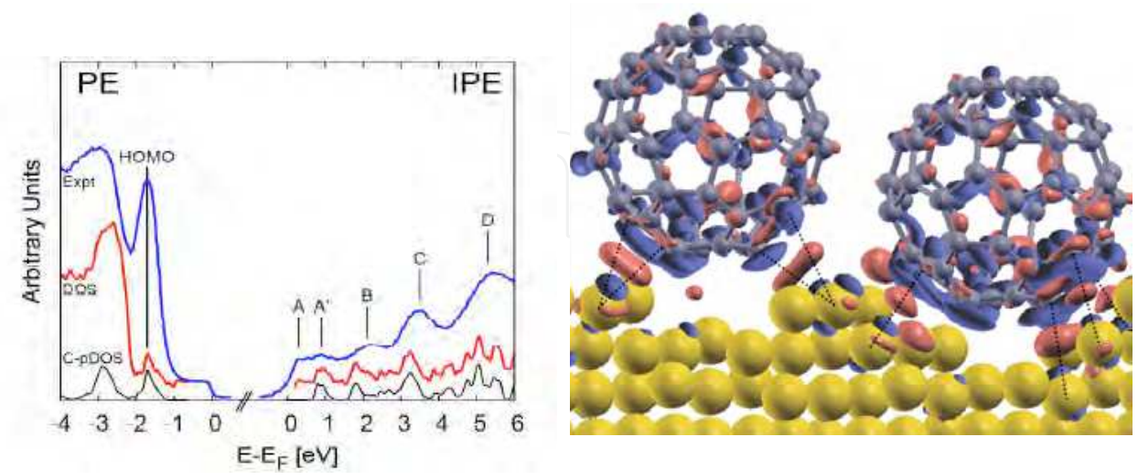

Fig. 18. Left: Comparison between experimental and calculated in-plane data corresponding to the C_{60}/Au(110)-p(6x5) surface reconstruction. The measured values and their associated uncertainties are proportional to the radii of the two empty semicircles. The filled semicircles are proportional to the calculated values using the final structure Right: Lateral views of the C_{60}/Au(110)-p(6x5) surface final structure. The observed corrugation has a height of one atomic level

4.2 Acenes on noble metals

Large acenes, C_{4n+2} H_{2n+4} (Figure 11 b) are conjugated organic molecules composed by *n* hexagonal rings, with H atoms, which saturate the frontier C orbitals. The π molecular states orientation is perpendicular to the molecular plane. Acenes form molecular crystals with triclinic structure showing polymorphism in the stacking d(001)-spacing (Mattheus 2001). In these crystals the electronic mobility is comparable with silicon (Schöhn 2000a in Mattheus 2001).

Thin films of tetracene (Tc, $C_{18}H_{10}$) and pentacene (Pn, $C_{22}H_{14}$), appear most promising candidates for the building of molecular organic semiconductors. Their transport properties in case of well-ordered thin films is highly anisotropic and is strongly influenced by the first layer structural, optical and electronic properties (Lukas, 2001, Söhnchen, 2004 Danişman, 2005, Käfer, 2007, Witte, 2004 and references therein).

The recent literature is quite rich on this topic. The bond of acenes on metals, have been revealed weaker than that of C_{60} on the same substrates. The presence of the H atoms at the molecular borders and their morphology reduce the possibility of hybridization with metal states. Different ordered phases are found for Tc and Pn adsorption on noble metals Pn/Au(111) (Witte 2004) (Schroder2003), Pn/Au(110) (Floreano2006, Badvek2008), Pn/Au(111) (Kafer 2007a, Duhm 2008), Pn/Ag(111),(Danişman 2005, Eremtchenko 2005, Pedio 2007, Kaefer2007b), Tc/Ag(111) (Langner et al. 2005) and in some cases the phase diagram appears complex.

As in other cases the growth mode of acenes is controlled by the nature of the substrate surface and the molecular orientation is determined by a competition of molecule-molecule vs molecule-substrate interactions. On noble metal surfaces acenes have a nearly flat orientation likely to allow the π conjugated molecular orbital to overlap at different degree with the metal electronic states, while on semiconductors acenes has the tendency to standing up. The orientation of pentacene molecules is controlled by the electronic structure of the substrate, namely the near-Fermi level density of states above the surface controls the interaction of the substrate with the pentacene π orbitals. A reduction of this density, as compared to noble metals, realized in semimetallic Bi(001) and Si(111)(5×2)Au surfaces, results in pentacene standing up (Thayer 2005).

The interaction of pentacene with metal surfaces has been studied extensively (Toyoda, 2010 and references therein) Pn/Cu(111) and Cu(110) (Lukas 2002, Lukas 2004). The intermolecular orientation onto noble metal surfaces, generally, adopts the preferred closed-packed side-by-side orientation Lukas 2002, Lukas 2004, but particular geometry of the substrate can induce a head-to head configuration (see for example Floreano, 2006). The film defects formation versus growth protocols and their effect on the subsequent grown layers, are widely discussed in the literature as well as the role of surface defects and stepped surfaces (Lukas 2001, Danişman 2005).

A recent DFT theoretical work relates the distance of the molecular plane of Pn from fcc (111) surfaces, with work function changes and the with hybridization of molecular states with substrate electronic properties. Calculation found that the Au(111) is rather "inert" to Pn layer, while pentacene interacting with Ag(111) and Cu(111) induces hybridization and a weak chemical bond. The sequence of the bond strength follows the Hammer Nørskov reactivity model (section 3). Similarly for the PTCDA molecule on (111) the strength of the bond follows the same trend (Duhm et al. 2008 b). On the other hand the interaction has been interpreted as mainly due to a redistribution of the metal substrate charge ("cushion" effect Witte 2005, Bredas 2010, Li 2009) drawn back by the deposition of weak adsorbates. This effect could lead to work function variations after acenes deposition, compatible with the experimental values on noble metals discussed by Baldacchini et al., 2006.

High Resolution photoemission of the Pn/Cu(119) and theoretical DFT results indicate that pentacene adsorbed on noble metals has the tendency to redistribute π states upon a weak "chemisorption" (Ferretti 2007).

For single layer of Pn/Cu(111) and Pn/Cu(110) the broadening of the NEXAFS features (Lukas, 2004) to was attributed to the electron coupling of the the molecular π orbital. Based on PES measurements, some kind of hybridization has been proposed for Pn/Cu(111) and Pn/Ag(111) (Jaeckel, 2008), while the molecule-substrate interaction for Pn/Au(111) is considered weaker.

Pn on Au(111) is an example of physisorptive organic/metal interface (Koch 2007). The interaction Pn_Au is weak, non-covalent and resulting from different contributions (Duhm2008). In case of Au(111) the Pn forms a variety of ordered phases, up to the completion of the single monolayer. The Au(111) herringbone reconstruction is still detectable by STM images (Schöder2003, Pong et al. 2009). The flat orientation (Käfer2007) of the first layer is related to a ΔW of 0.95 eV and to the formation of an intermolecular dipole

modelled by an electrostatic model. The existence of a surface dipole built into molecular layers is conceptually different from the surface dipole at metal Surfaces. Its origin lies in the details of the molecular electronic structure and its magnitude depends on the orientation of molecules relative to the surface of an ordered assembly.

The analysis of the dependence by incident light polarization of C K-edge NEXAFS of the 1 ML Pn on Ag(111) indicate that the Pn molecule is chemisorbed with a tilt angle of 10°+/- 5°. Higher tilt angle 25°+/- 5° were found for submonolayer coverages. This deformation of the LUMO with respect to the LUMO transitions in gas phase Pn (Alagia, 2005) is present for coverages close to the single layer (Figure 19, Pedio2007). This framework in the Pn/Ag(111) is also suggested by (Kaefer 2007b). The electronic π molecular states changes across this orientation transition. XAS spectra show a redistribution of the oscillator strength in the C 1s LUMO excitations as a function of the Pn coverage, together with modifications of the density of states in the filled HOMO region.

Valence band UPS and NEXAFS spectroscopies applied to Tc and Pn adsorption on Ag(111) and Au(111), from subML to 1 ML coverages, show differences in the HOMO and LUMO states related to a redistribution of the molecular states (Pedio, 2008). From NEXAFS, LUMO results strongly modified in the cases of Tc and Pn deposited on Ag(111) substrate and less perturbed on Au(111).

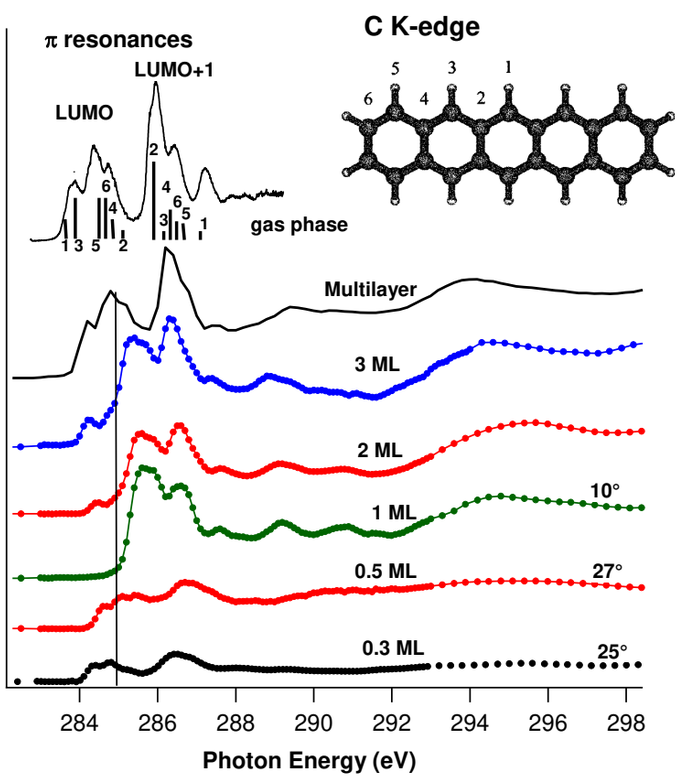

Fig. 19. C K edge XAS of Pentacene on Ag(111) at different molecular coverages in monolayer taken at the magic angle (Pedio 2007). Gas phase spectrum is shown (top); the bars indicate the calculated contributions from different inequivalent C atoms (see numbers in the sketch of pentacene molecule).

Further work is in progress to understand the hybridization degree and the dispersion of the molecular states of the various presented systems. In any case we can indicate a progression of the bond from the stronger Pn/Ag(111) to the weaker Tc/Au(111) (Pedio, 2008). The modification of the HOMO and LUMO molecular states confirms the trend found by DFT (Toyoda 2010) and supporting the modification of the π molecular states of adsorbed acenes on the Ag(111) substrate and the weaker interaction with Au(111).

A peculiar case is the Pn/Au(110). Even in this case the phase diagram is complex (Figures 20 and 21). A multitechnique approach permitted to determine the molecular orientation of the 6x3, 3x6 and 6x8 phases.

The phase diagram indicates that that two-dimensional commensurate growth only occurs in the monolayer range for a substrate temperature, *T*s, higher than about 370 K. The highest coverage ordered phase displays a (6 x 8) symmetry and corresponds to the saturation coverage at *T*s = 420 K. The (3 x 6) phase corresponds to the saturation coverage of the first layer at *T*s =470 K. Helium scattering (HAS) experiments provide information similar to the S-XRD. Figure 20 shows HAS along the [001], ΓY, direction collected at RT after deposition at *T*s = 420 K for the (6 x8) phase (filled triangles) and *T*s = 470 K for the (6 x 3) and (3 x 6) phases (open circles and filled squares, respectively). The 2-fold symmetry pattern of the clean missing row reconstructed substrate is also reported at the bottom of the graphic (full line). As a guide to the eye, fractional peaks of the eighth order are indicated at the bottom *x* axis, while fractional peaks of the sixth order are reported at the top *x* axis.

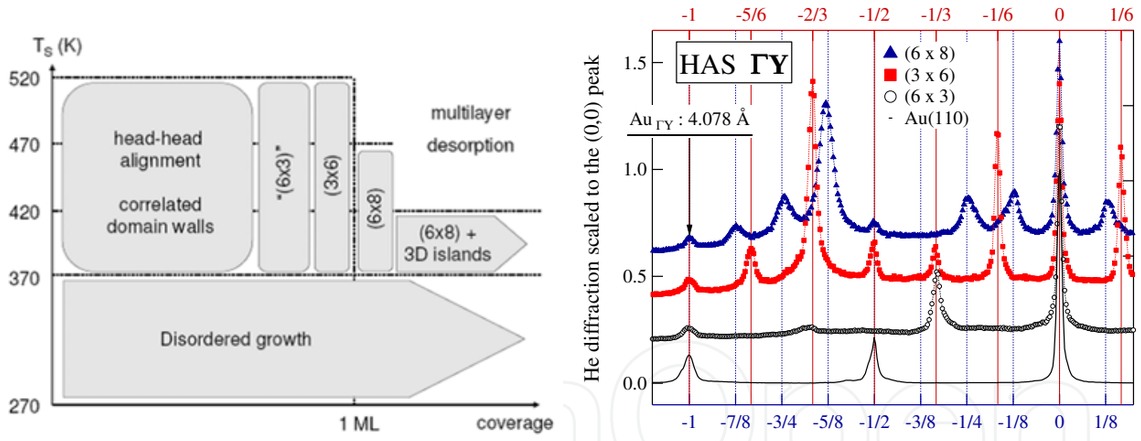

(a) (b)

Fig. 20. a) Phase diagram of pentacene films on Au(110). The (6 x 3) phase is quoted since it has not a well defined equilibrium coverage. The completion of the first monolayer is conventionally assigned between the (3 x 6) and (6 x 8) phases. In figure b are shown the peaks of the different ordered phase

The models of the systems were obtained by means of HAS (Floreano, 2006), NEXAFS and STM (Badvek, 2008). In the monolayer range, pentacene forms two commensurate phases with (3 x 6) and (6 x 8) symmetry. The (3 x 6) phase only contains equivalent, perfectly flat molecules that are aligned side-by-side along [001], thus forming crosstie chains extending along the $\left[1\bar{1}0\right]$ direction. These chains are also preserved in the high coverage (6 x 8)

phase, but they display a wider separation since new chains are accommodated in between, with the additional molecules aligned head-to-tail along the $[1\bar{1}0]$ direction and tilted by approximately 90° around their molecular axis. This structure, formed by three molecules per unit cell (two flat and one tilted), forms large domains of nanorails.

In fig. 20 the HAS measurements shows the disappearing of the ½ peak of the gold reconstruction indicating a deconstruction of the Au(110) missing row caused by the molecular deposition. This has been also confirmed by preliminary SXRD results[4].

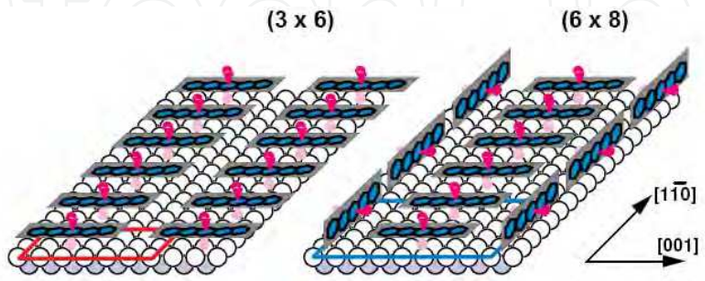

STM

Fig. 21. Models of the 3x6 and 6x8 Pn/Au(110) reconstruction, based on He scattering, STM and NEXAFS measurements. The directional pai states of the Pn are presented in red.

These results enlighten the local rearrangement of the charge at the interface. A possible depletion of electron charge in correspondence of the new chains, inducing an upstanding orientation of Pn, can be inferred.

4.3 Porphyrine derivatives on noble metals

Porphyrine derivatives constitute the essential functional units for many processes and Nature demonstrates their great functionality, variability and chemical stability in many cases. Metalloporphyrin are base components of biological molecules as chlorophyll (Mn porphyrin), emoglobin (Fe porphyrin) and are efficient in the Oxygen exchange.

They are formed by a macrocycle and surrounding groups (Fig. 11 right). The central porphine ring is composed by 4 Pyrrole rings linked by methine bridges (porphyrins) or N (Phtalocyanins). By varying the choice of the metal center, the bonding and characteristics of the metalloporphyrin or the phtalocyanine may be dramatically affected. This is reflected in spectroscopic measurements as XPS and XAS.

A clear description of the electronic properties of porphirinoids is still under debate in the literature, due to the high degree of variation in the simulations. The energy sequence of the valence and conduction electronic states show discrepancies, indicating that the energy ordering in metal-organic molecules crucially depends on the electronic solution employed and the functional theory adopted (Stenuit et al., 2010, Maron et al. 2008).

Porphyrins films grown by various methods (UHV vapour deposition, solutions etc) received a paramount interest and the literature is extremely rich. New interesting results have been achieved recently, as for example a Kondo effect related to the spin of the central atom in Co and Fe phtalocyanines on Au(111), the induced magnetic order of Mn

[4] L.Floreano privat communication

porphyrins on Co films as well as magnetic coupling effects (Wende et al. 2007 cited in Fanetti et al. 2011). Recently in the CoEOP deposited onto Ag(110) (Fanetti et al 2011), a charge transfer to the LUMO orbital has been found. DFT calculations indicate that the molecular interaction with the substrate leads to the electron transfer from the Ag substrate to the molecule. This can be responsible of the steric adsorption of the CoOEP, that results titled of 15°, at variance with other similar systems.

Porphyrins can be deposited in highly ordered single monolayers on metal surfaces, leading to ordered structures. Covalent interaction between the central metal atom and substrates, the "Cushion" effect induced at the noble metal surface, and the out-of-plane central atom dipole moments plays a role in the different cases. No clear trend, as a function of external group, central metal atom element and substrate element and structure, is still available.

On the noble metal (111) surfaces, and often on the (100) planes, both porphyrins and phtalocyanines are found to lay in a planar-like configuration presenting large terraces domains. In case of Au(111) substrates, the herringbone reconstruction remains detectable. The long range ordening of these "floating" molecular layers show dependency on the substrate element and on the kind of porphyrinoid and central metal atom. For example differences between single layers Cu and Ni octaethylporphyrins deposited on Au(111) have been detected in the diffraction patterns and in the electronic properties (Resta et al. 2010).

The interaction with (110) substrates appears different. Restructuring has been indicated by STM in case of Cu-phtalocyanine (CuPc) deposited on Ag(110) (ref. Bohringer et al. 1997 cited in Rosei et al. 2003). CuPc induces a transition from thermodynamically controlled 3-dimensional faceting at submonolayer coverage, to a kinetically dominated 2-dimensional step faceting process, when coverage approaches a full monolayer. Transition metal-phtalocyanine on Au(110) surfaces result regularly spaced. High Resolution PES show interface electronic states close to the Fermi level. Their energies are different from CuPc to FePc and CoPc molecules. Structurally CuPc on Au(110) present a complex phase diagram with strong mass transport of the substrate as a function of the molecular coverage from submonolayer to the 1 ML (Floreano 2008). Again the molecular deposition deconstructs the Au missing row and a set of higher periodicities (x5, x3, x7) are progressively detected along the [001] direction. In conclusion coverage-dependent transformation on fcc 110 substrates seems to be driven by the molecule−substrate interaction. This interaction seems to take place in other porphyrinoid deposited onto fcc (111) substrates but, in any case it appears such that no mass transport of these substrate takes place.

Due to the complexity of the roles played, in the balance among interactions, by the central metal atom in the porphyn ring, by the external groups and frontier orbitals, and by the interaction with the metal substrates (polarization, dipoles etc.), a complete understanding of these systems deserve further study.

Note, finally, that in some cases the molecular morphology results altered by STM (Donovan et al. 2010).

5. Conclusions

Noble metal surfaces offer a variety of structural/electronic moieties which can be used in the organic-inorganic engineering. The comparisons of the similarities and differences of the (111) and (110) surfaces show how the charge reservoir of isotropic or anisotropic electron

density guides the interaction, from charge transfer to directional bonds, between molecules and substrate.

Noble metal surfaces are valuable substrates for building self assembled organic thin layers because of their:

- Low chemical reactivity together with high atomic surface mobility resulting in the capability of reordering after molecular deposition. Often order is thermally activated.
- Good degree of morphological order of the crystal surfaces
- Guide for the molecular ordering through the symmetry of the surface. If commensurable the overlayer must follow the substrate symmetry. In case the intermolecular interactions prevail, in strength, compared to the molecular-structural the layer can by uncommensurate.
- High electron density at the crystal surface (in case of (111) in Au, Ag and Cu the electrons form a quasi-two-dimensional gas at surface) providing a charge reservoir.

The details of interaction are crucial for the functionalization of the molecular films.

The anchoring of the molecules is due to a combination of effects (Rosei 2005): i) Adaptation of the surface geometry Larger interaction area, that allows to the molecule to fit into the local structure of substrates ; ii) Higher reactivity of the substrate (stronger bond) facilitates the creation of nanodimple sites underneath the molecules. A simple correlation exists between the bonding strength of a molecule and the metal coordination number of the adsorption site *d* -band model by Hammer and Nørskov. iii) The adsorption inducing restructuring is typically thermally activated: it provides an Energy gain in the adsorption energy ΔE_{ad} of the molecules on the reconstructed surface, balancing the energy cost ΔE_{metal} required to break the metal bonds

The formation of directional bonds seems the base mechanism for the nanopit formation, at least for strong chemisorbed species (as fullerene). C60 induced reconstruction of substrates is thermally activated, even on the close packed fcc (111) surfaces. The molecule results locally perturbed with the electronic properties (particularly the LUMO orbitals), that are modified by the interaction. The structural characterizationof the molecules onto the (110) substrate demonstrates the formation of NANOPITS and/or FACETTING of the metal surface.

In case of "flat" and conjugated molecules, as acenes and prophyrin derivatives, the interrelations of the various aspects (morphology, dipoles-electrostatic configuration at interfaces, distribution of the charge of the metal substrate etc…) are particularly evident. Molecular orientation, long range ordening, surface reconstruction and charge (re)distribution (interface dipole, molecular dipole, "cushion" effect) are all present at different but never negligible degree, depending on the chosen molecule and on the substrate morphology/surface energy/reactivity.

6. References

Africh C. 2011. Surface Structure and Reactivity laboratory CNR-IOM, TASC Available from: www.tasc.infm.it

Alagia, M.; Baldacchini, C. Betti, M. G. Bussolotti, F. Carravetta, V. Ekström, U.; Mariani, C. & Stranges S. (2005). Core-shell photoabsorption and photoelectron spectra of gas-

phase pentacene: experiment and theory. *J Chem. Phys* Vol. 122, No. 12 (22 March 2005), pp. 124305

Ashcroft, N. W. & Mermin, N. D. (1976). Solid State Physics. Saunders College, HRW ISBN 0-03-083993-9

BALSAC Available from: http://www.fhiberlin.mpg.de/~hermann/Balsac/pictures.html

Bassani, F. & Altarelli M. (1983). Interaction of radiation with condensed matter, In *Handbook on Synchrotron Radiation,* Vol. I, E.E. Koch (Ed), 463-605, North-Holland Publishing Company Amsterdam (1983).

Baldacchini, C.; Mariani, C. Betti, M. G. Gavioli, L. Fanetti, M. & Sancrotti, M. (2006). Molecular gap and energy level diagram for pentacene adsorbed on fille d-band metal surfaces. *Appl. Phys. Lett* Vol. 89, 2006. pp. 152119 1 -3

Bavdek, G.; Cossaro, A. Cvetko, D. Africh, C. Blasetti, C. Esch, F. Morgante, A. & Floreano, L. (2008). Pentacene Nanorails on Au(110). *Langmuir* Vol. 24 (No. 3), (December 2007), pp 767–772.

Benfatto, M. & Felici, R. (2001). Resonant atomic scattering factor theory: A multiple scattering approach:*Phys. Rev. B* Vol. 64, No.11 (24 August 2001) 115410 (9 pages).

Brühwiler, P.; Karis, A. O. & Mårtensson N. (2002). Charge-transfer dynamics studied using resonant core spectroscopies. *Review of Modern Physics*, Vol. 74, (2002). pp. 703-740

Besenbacher, F. (1996). Scanning tunnelling microscopy studies of metal surfaces, *Rep. Prog. Phys. Vol.* 59 (1996), pp. 1737–1802

Chen C. (1993). *Introduction to Scanning Tunneling Microscopy* . Oxford University Press.

Cepek, C.; Goldoni, A. Modesti, S. (1996). Chemisorption and fragmentation of C_{60} on Pt(111) and Ni(110). *Phys. Rev. B* Vol. 53, (March 15, 1996)pp. 7466– 7472 Available from: http://link.aps.org/doi/10.1103/PhysRevB.53.7466

Cepek, C.; Giovanelli, L.; Sancrotti, M.; Costantini, G.; Boragno, C.& Valbusa U. (2000). Electronic structure and growth mode of the early stages of C60 adsorption at the Ag(001) surface. *Surf. Sci.* Vols. 454-456, pp. 766-770

Cepek, C.; Sancrotti, M. Greber T. & Osterwalder J. (2000). Electronic Structure of K doped C60 monolayers on Ag(001) *Surf. Sci.* Vols. 454-456, (2000) pp. 467–471

Cepek, C.; Vobornik, I. Goldoni, A. Magnano, E. Selvaggi, G. Kröger, J. Panaccione, G. Rossi, G. & Sancrotti M. (2001). Temperature-Dependent Fermi Gap Opening in the c(6×4)–C_{60}/Ag(100) Two-Dimensional Superstructure. *Phys. Rev. Lett.* Vol. 86, (April 2, 2001) pp. 3100-3102 Available from: http://link.aps.org/doi/10.1103/PhysRevLett.86.3100

Clark, D.E.; Unertl, W.N. & Kleban P.H. (1986). Specific-heat anomaly of Au(110) (1 × 2) studied by low-energy electron diffraction *Phys. Rev. B* Vol. 34 No. 6 (1986) pp. 4379-4381.

Danişman, M. F.; Casalis, L. & Scoles, G. (2005). Supersonic molecular beam deposition of pentacene thin films on two Ag(111) surfaces with different step densities. *Phys. Rev. B* Vol. 72 pp. 085404.

Donovan, P.; Robin, A.; Dyer, M. S. Persson, M. & Raval, R. (2010). Unexpected Deformations Induced by Surface Interaction and Chiral Self- Assembly of CoII-Tetraphenylporphyrin (Co-TPP) Adsorbed on Cu(110):A Combined STM and Periodic DFT Study. *Chem. Eur. J.* vol. 16, (2010) pp. 11641 – 11652 Available from: http://dx.doi.org/10.1002/chem.201001776

Dose, V. (1985). Momentum-resolved Inverse Photoemission. *Surf. Sci. Rep* Vol. 5, No. 8 (1985), pp. 337-378. Available from:

http://www.sciencedirect.com/science/article/pii/0167572985900068

Duhm, S.; Heimel, G.; Salzmann, I.; Glowatzki, H.; Johnson, R. L.; Vollmer, A.; Rabe, J. P. & Koch, N. (2008). Orientation-dependent ionization energies and interface dipoles in ordered molecular assemblies. *Nature Materials*, Vol. 7, pp. 326-330

Duhm, S; Gerlach, A.; Salzman, I.; Broeker, B.; Johnson, R.L.; Screiber, F. & Koch, N. (2008). b) PTCDA on Au(111), Ag(111) and Cu(111):Correlation of interface charge transfer to bonding distance. *Organic Electronics.* Vol. 9 pp. 111-118

Eremtchenko, M.; Temirov, R.; Bauer, D.; Schaefer, J. D. & Tautz F. S. (2005). Formation of molecular order on a disordered interface layer: Pentacene/Ag(111). *Phys. Rev. B* Vol. 72, No. 11 pp. 115430 (9 pages).

Fall, C.J.; Bingelli, N. & Baldereschi, A. (2000). Work-function anisotropy in noble metals: Contributions from d states and effects of the surface atomic structure. *Phys. Rev. B* Vol. 61, No. 12, pp. 8489–8495.

Feidenhans'l, R. (1989). Surface Structure Determination by X-ray Diffraction. *Surf.Sci Rep.*, Vol. 10, pp. 105-188.

Hammer, B. (2006). Special sites at Noble and late transition metal catalysts. *Chemistry and Material Science, Topics in Catalysis*, Vol. 37, No.1, pp. 3-16.

Hinterstein, M.; Torrelles, X. Felici, R. Rius, J. Huang, M. Fabris, S. Fuess, H. & Pedio, M. (2008). Looking underneath fullerenes on Au(110): Formation of dimples in the substrate, Phys Rev B Vol. 77 No. 15, (2008) pp. 153412 (4 pages), also selected in Virtual Journal of Nanoscale Science & Technology vol 17, May 12, 2008 issue 19.

Hüfner, S. (1995). *Photoelectron Spectroscopy Principles and applications*. Springer Berlin ISNB 3-540-19108-9

Käfer, D; Ruppel, L. & Witte, G. (2007). a). Growth of pentacene on clean and modified gold surfaces. *Phys. Rev. B.* Vol. 75 pp. 085309. Available from: http://link.aps.org/doi/10.1103/PhysRevB.75.08530

Käfer, D. & Witte, G. (2007). b). Evolution of pentacene films on Ag(111): Growth beyond the first monolayer. *Chem. Phys. Lett.* Vol. 442. (June 2007) pp. 376-383

Koch, N.; Vollmer, A. Duhm, S. Sakamoto, S. Suzuki, Y. (2007) The Effect of Fluorination on Pentacene/Gold Interface Energetics and Charge Reorganization Energy. *Adv. Mater. Vol.* 19, (January 2007) pp.112-116.

Fanetti, M. Calzolari, A. Vilmercati, P. Castellarin-Cudia, C. Borghetti, P. Di Santo, G. Floreano, L. Verdini, A. Cossaro, A. Vobornik, I. Annese, E. Bondino, F. Fabris, S. Goldoni, A. (2011). The Structure and the Molecule-Substrate Interaction in a Co-Octaethyl Porphyrin Monolayer on the Ag(110) Surface. *J. Physical Chemistry* C in press. Manuscript ID: jp-2011-011233

Felici, R.; Pedio, M. Borgatti, F. Iannotta, S. Capozi, M. Ciullo, G. Stierle, A. (2005). X-ray diffraction characterization of Pt(111) surface nanopatterning induced by C_{60} adsorption. *Nat. Mat.* Vol 4 (September2005) pp.688-692.

Felici R. & Pedio M. (2009). Nanostructure induces by the adsorption of fullerenes: structural and Electronic properties review paper in Proceedings of the Workshop Synchrotron Radiation and Nanostructures, Papers in Honour of Paolo Perfetti eds A. Cricenti and G. Margaritondo pp. 209-223 (2009), Word Scientific New Jersey, ISBN-13 978-981-4280-83-9

Ferretti, A.; Baldacchini, C. Calzolari, A. Di Felice, R. Ruini, A. Molinari, E. & Betti M. G. (2007). Mixing of Electronic States in Pentacene Adsorption on Copper. *Phys. Rev. Lett.* Vol. 99 No. 4, July 25, 2007 pp. 046802 (4 pages).

Floreano, L.; Cossaro, A. Cvetko, D. Bavdek, G. & Morgante A Phase Diagram of Pentacene Growth on Au(110). (2006). *J. Phys. Chem. B*, 110 (10), (February 17, 2006) pp 4908–4913.

Floreano, L.; Cossaro, A. Gotter, R. Verdini, A. Bavdek, G. Evangelista, F. Ruocco, A. Morgante, A. & Cvetko, D. (2008). Periodic arrays of Cu-Phthalocyanine chains on Au(110), *J. Phys. Chem. C* Vol. 112 (2008) pp.10794.2008.

Gavioli, L. & Cepek, C. (2008). Ultrathin Fullerene-Based films via STM and STS. In: Applied Scanning Probe Methods (Eds) Bhushan B; Fuchs, H & Tomitori,M. series Nanoscience and Technology, 2008 Sprinter-Verlag Berlin.

Gargiani, P.; Angelucci, M. Mariani, C. & Betti M. G. (2010). Metal-phthalocyanine chains on the Au(110) surface: Interaction states versus *d*-metal states occupancy. *Phys. Rev. B* Vol. 81, No. 8 pp. 085412 (7 pages).

Giudice, E.; Magnano, E. Rusponi, S. Boragno, C. & Valbusa, U. (1998). Morphology of C_{60} thin films grown on Ag(001) *Surf. Sci.* Vol. 405 No. 2-3 (5 May 1998) pp. L561-565.

Goldoni A. Cepek C. Magnano E. Laine A. D. Sancrotti M. (1998). Temperature dependence of the electronic structure near E_F and electron-phonon interaction in C60/Ag(100) single layers. *Phys. Rev. B* Vol. 58 No. 4, pp. 2228-2332

Li, H.; Duan, Y. Coropceanu, V. & Bredas J-L. (2009). Electronic structure of the pentacene-gold interface: a density-functional theory study. *Organic Electronics* Vol. 10 pp. 1571-1578.

Langner, A.; Hauschild, A. Fahrenholz, S. & Sokolowski, M. (2005). Structural properties of tetracene films on Ag(1 1 1) investigated by SPA-LEED and TPD. *Surf Sci* Vol. 574 (10 November 2004) pp. 153-165.

Li, H. L. ; Pussi, K. Hanna, K. J. Wang, L.-L. Johnson, D. D. Cheng, H.-P. Shin, H. Cuartarolo, S. Moritz, W. Smerdon, J. A. Mc.Grath, R. & Diehl R. D.. 2009. Surface Geometry of C_{60} on Ag(111). *Phys. Rev. Lett.* Vol. 103 No. 5, pp. 056101 (4 pages).

Lu, X.; Grobis, M. Khoo, K. H. Louie, S. G. & Cromie M. F. (2003). Spatially Mapping the Spectral Density of a Single C60 Molecule. *Phys. Rev. Lett.* Vol. 90 No.9, 096802 (4 pages).

Lukas, S.; Vollmer, S. Witte, G. &Woll Ch. (2001). Adsorption of acenes on flat and vicinal Cu(111) surfaces: Step induced formation on lateral order. *J.Chem. Phys* Vol. 114, No. 22, pp. 10123-10130.

Lukas, S.; Witte, G. & Wöll Ch. (2002) Novel Mechanism for Molecular Self-Assembly on Metal Substrates: Unidirectional Rows of Pentacene on Cu(110) Produced by a Substrate-Mediated Repulsion *Phys. Rev. Lett.* Vol. 88, No. 2 (December 28, 2002) pp. 028301 (4 pages).

Lukas, S.; Söhnchen, S. Witte, G. & Wöll Ch.. (2004). Epitaxial growth of pentacene films on metal surfaces. *Chem.Phys.Chem* Vol. 5 pp. 266-270.

Lüth, H. (1996) Surfaces and Interfaces of Solid Materials, Springer Berlin. ISBN 3-540-58576-1 3.

Marom N.; Hod, O. Scuseria, G. E. & Kronik L. 2008. Electronic structure of copper phthalocyanine: A comparative density functional theory study. *J. Chem. Phys.* Vol. 128, No. 16. pp. 164107-(6 pages).

Mattheus, C. C.; Dros, A. B. Baas, J. Meetsma, A. de Boer, J. L. & Palstra T.M. Polymorphysm in pentacene. (2001) *Acta Crystallographica Section C Crystal Structure Communications* Vol. C57 pp. 939-941. ISSN 0108-2701.

Maxwell, A. J.; Brühwiler, P. A. Nilsson, A. Mårtensson, N. & Rudolf P. (1994). Photoemission, autoionization, and x-ray-absorption spectroscopy of ultrathin-film C_{60} on Au(110). *Phys. Rev. B* Vol. 49 No. 15, (April 15, 1994) pp. 10717 –10725.

NIST X-ray Photoelectron Spectroscopy Database 20, version 3.4 (Web version), http://srdata.nist.gov/xps/

Nickel, B.; Fiebig, M. Schiefer, S. Göllner, M. Huth, M. Erlen, C. & Lugli P. (2008). Pentacene devices: Molecular structure, charge transport and photo response *Phys. Stat.Sol. (a)* pp. 205, No. 3, pp. 526–533.

Pedio, M.; Hevesi, K. Zema, N. Capozi, M. Perfetti, P. Gouttebaron, R. Pireaux, J.-J. Caudano R. & Rudolf, P. (1999). C_{60}/metal surfaces: adsorption and decomposition. *Surf. Sci.* Vol. 437, (June 1999) pp. 249- 260.

Pedio, M.; Felici, R. Torrelles, X. Rudolf, P. Capozi, M. Rius, J. & Ferrer S. (2000). Study of C_{60}/Au(110)-p(6×5) Reconstruction from In-Plane X-Ray Diffraction Data *Phys. Rev. Lett.* Vo. 85 No. 5, pp. 1040-1043.

Pedio, M.; Doyle, B. Mahne, N. Giglia, A. Borgatti, F. Nannarone, S. Johansson, S. Temirov, R. Tautz, S. Casalis, L. Hudej, R. Danisman, M.F. & Nickel B. (2007). Growth of Pentacene on Ag(111) surface: A NEXAFS study. *Applied Surface Science* Vol. 254, pp. 103-107

Pedio, M.; Doyle, B. Mahne, N. Giglia, A. Nannarone, S. Montecchi, M. Pasquali, L. (2008). *J. Phys.: Conf. Ser.* Molecular states of polyacenes grown on noble metal surfaces. Vol. 100 pp. 052072 1-4, IVC-17/ICSS-13 and ICN+T2007 Lund July 2007. Available from: http://iopscience.iop.org/1742-6596/100/5/052072/

Pong, I. F.; Yau, S. Huang, P-Y. & Chen, M.-C. (2009). In situ STM Imaging of the Structures of pentacene Molecules adsorbed on Au(111). *Langmuir*, Vol 25, No 17 (November 2009) pp. 9887-9893.

Resta, A.; Felici, R. Kumar, M. & Pedio M., (2010). Ni and Cu octaethyl porphyrins ordered monolayer on Au(111) surfaces. *Journal of Non-Crystalline Solids* Vol. 356 pp. 1951–1954.Robinson, I.K. (1986). Crystal truncation rods and surface roughness. *Phys. Rev. B* Vol. 33, No. 6, (march 1986), pp. 3830-3836.

Robinson, K. & Tweet D. J. (1992). Surface X-ray diffraction. *Rep. Prog. Phys.* Vol. 55, pp. 599-651. Available from: http://iopscience.iop.org/0034-4885/55/5/002.

Rosei, F.; Schunack, M. Naitoh, Y. Jiang, P. Gourdon, A. Laegsgaard, E. Stensgaard, I. Joachim, Ch. & Besenbacher F. 2003. Properties of Large organic molecules on metal surfaces. *Progress in Surface Science* Vol. 71, pp. 95-146.

Sandy, A.R.; Mochrie, S.G.J. Zehner, D.M. Huang, K.G. & Gibbs D. (1991). Structure and phases of the Au(111) surface: X-ray-scattering measurements. *Phys Rev B* Vol. 43 No. 6, (15 feb 1991) pp. 4667- 4687.

Schöder, P. G.; France, C. B. Park, J. B. & Parkinson B. A. (2003). Orbital Alignment and Morphology of Pentacene Deposited on Au(111) and SnS2 Studied Using Photoemission Spectroscopy . *J. Phys. Chem. B* Vol. 107. No. 10 (February 2003) pp. 2253-2261

Scudiero, L.; Barlow, D.E. & Hipps, K.W. (2002). Scanning Tunneling Microscopy, Orbital Mediated Tunneling Spectroscopy, and Ultraviolet Photoelectron Spectroscopy of Nickel(II) Octaethylporphyrins Deposited from vapor. *J. Phys. Chem. B*, Vol. 106, pp. 996-1003.

Singh-Miller, N. E. Marzari, N. (2009). Surface energies, work functions, and surface relaxations of low-index metallic surfaces from first principles. *Phys Rev. B* Vol. 80 No. 23 (2009) pp. 235407 (9 pages).

Smoluchowski, R. (1941). Anisotropy of the Electronic Work Function of Metals. *Phys. Rev.* Vol. 60, No. 9 pp. 661-674 . ISSN 0031899X.

Söhnchen, S.; Lukas, S. & Witte, G. (2004). Epitaxial growth of pentacene films on Cu(110). *J. Chem. Phys.* Vol. 121, pp. 525. Available from: http://jcp.aip.org/resource/1/jcpsa6/v121/i1/p525_s1

Stenuit, G.; Castellarin-Cudia, C. Plekan, O.K. Feyer, V. Prince, K.C. Goldoni, A. & Umari, P. (2010). Valence electronic properties of porphyrin derivatives. *Phys Chem Chem Phys* Vol. 12, No. 36, pp. 10812 (7 pages). Available from: http://pubs.rsc.org/en/content/articlelanding/2010/cp10.1039/c004332j

Stöhr, J. (1992). NEXAFS Spectroscopy, Springer-Verlag Berlin ISBN 3-540-54422-4

Stolze, P. (1994). Simulation of surface defects. *J. Phys::Condens. Matter* Vol 6 (1994) pp. 9495-9517

Toyoda, K.; Hamada, I. Lee, K. Yanagisawa, S. & Morikawa, Y. (2010). *J. Chem. Phys.* Vol. 132 pp. 134793 (9 pages).

Thayer, G.E.; Sadowski, J. T. Meyer zu Heringdorf, F. Sakurai, T. & Tromp R. M. (2005). *Phys. Rev. Lett.* Vol. 95, No.25 pp. 256106 (9 pages).

Triguero, L.; Pettersson, L.G. M. & Ågren, H. (1998). Calculations of near-edge x.ray absorption spectra of gas-phase and chemisorbed molecules by means of density-functional and transition-potential theory. *Phys. Rev. B* Vol. 58, No.12 pp. 8097-8110.

Vitos, L.; Ruban, A. V. Skiver, H.L. & Kollàr, J. (1998). The Surface energy of metal. *Surf. Sci.* Vol. 441, No. 1-2 (August 1998) pp. 186-202. Available from: http://www.sciencedirect.com/science/article/pii/S003960289800363X

van Hove, M. A.; Koestner, R. J. Stair, P. C. Biberian, J. P. Kesmodel, L. L. Bartos, I. & Somorjai, G. A. (1981). The surface reconstructions of the (100) crystal faces of iridium, platinum and gold: I. Experimental observations and possible structural models. *Surf. Sci.* Vol. 103, No.1. (1 feb 1981), pp. 189-217.

Vlieg, E.; (2000). ROD: a program for surface X-ray crystallography *J. Appl. Cryst.* Vol. 33, pp. 401- 405. ISSN 0021-8898

Witte G. & Wöll Ch. (2004). Growth of aromatic molecules on solid substrates for applications in organic electronics *J. Mater. Res.* Vol. 19, No. 7, pp. 1889- 1916 and references therein.

Witte, G.; Lukas, S. Bagus, P.S. & Wöll, Ch. (2005). Vacuum level alignment at organic/metal junctions:"Cushion" effect and the interface dipole. *Appl. Phys. Lett.*Vol. 87 pp. 263502 (3 pages).

Werner W. *Tutorial on Electron Spectroscopies*. 20.10.2011. Available from: http://eaps4.iap.tuwien.ac.at/~werner/qes_tut.html#main

Woodruff, D. P. & Delchar, T. A. (1988). *Modern Techniques of Surface Science*. Cambridge University Press ISBN 0 521 35719 5.

Zahn, D. R.T.; Gavrila, G. N. & Gorgoi M. (2006). The transport gap of organic semiconductors studied using the combination of direct and inverse photoemission. *Chemical Physics* Vol. 325 pp. 99–112

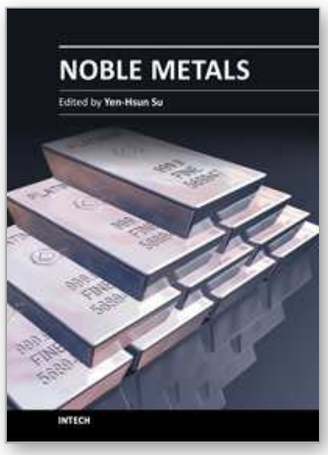

Noble Metals

Edited by Dr. Yen-Hsun Su

ISBN 978-953-307-898-4
Hard cover, 426 pages
Publisher InTech
Published online 01, February, 2012
Published in print edition February, 2012

This book provides a broad spectrum of insights into the optical principle, resource, fabrication, nanoscience, and nanotechnology of noble metal. It also looks at the advanced implementation of noble metal in the field of nanoscale materials, catalysts and biosystem. This book is ideal not only for scientific researchers but also as a reference for professionals in material science, engineering, nonascience and plasmonics.

How to reference

In order to correctly reference this scholarly work, feel free to copy and paste the following:

Maddalena Pedio, Cinzia Cepek and Roberto Felici (2012). Organic Molecules on Noble Metal Surfaces: The Role of the Interface, Noble Metals, Dr. Yen-Hsun Su (Ed.), ISBN: 978-953-307-898-4, InTech, Available from: http://www.intechopen.com/books/noble-metals/organic-molecules-on-noble-metal-surfaces-the-role-of-the-interface

INTECH
open science | open minds

InTech Europe
University Campus STeP Ri
Slavka Krautzeka 83/A
51000 Rijeka, Croatia
Phone: +385 (51) 770 447
Fax: +385 (51) 686 166
www.intechopen.com

InTech China
Unit 405, Office Block, Hotel Equatorial Shanghai
No.65, Yan An Road (West), Shanghai, 200040, China
中国上海市延安西路65号上海国际贵都大饭店办公楼405单元
Phone: +86-21-62489820
Fax: +86-21-62489821

IntechOpen